RSC Sustainability

ROYAL SOCIETY OF CHEMISTRY

TUTORIAL REVIEW

View Article Online
View Journal | View Issue

Cite this: *RSC Sustainability*, 2025, **3**, 2806

Loofah sponge: a sustainable material for wastewater desalination

Susmi Anna Thomas, *[a] Jayesh Cherusseri *[b] and Deepthi N. Rajendran *[a]

Received 19th January 2025
Accepted 8th April 2025

DOI: 10.1039/d5su00043b

rsc.li/rscsus

Treatment of wastewater has become a necessity to address the shortage of drinking water in this era due to population explosion as well as shortage of water resources. It is necessary to develop wastewater treatment approaches that are facile, eco-friendly, scalable, and low cost. Among the various choices available to date, desalination is a versatile and suitable method which involves an interfacial evaporation of salt ions from seawater to produce freshwater. The desalination method involves a membrane-based process in which the development of suitable and cost-effective ways is a prerequisite. There have been many membranes developed in the recent past including carbon-based membranes (such as graphene membranes, graphene oxide membranes, *etc.*), MXene-based membranes, *etc.* Among the various available choices, biomass-based materials have become attractive to develop membranes which are economically feasible and environmentally friendly materials that can be produced on a large scale. By considering the advantageous features of biomass-based materials, water desalination becomes a cost-effective approach for the present

[a]*Department of Physics, Government College for Women (Affiliated to University of Kerala), Thiruvananthapuram, Kerala 695014, India. E-mail: deepthinrphysics@gmail.com*

[b]*Department of Chemistry (BK21FOUR), Research Institute of Advanced Chemistry, Gyeongsang National University, Jinju 52828, Republic of Korea. E-mail: drjayeshpuli@gmail.com*

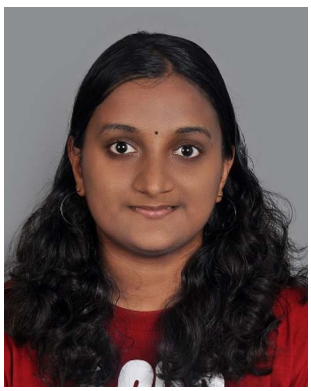

Susmi Anna Thomas

Susmi Anna Thomas is a PhD scholar at the Department of Physics, Government College for Women, Thiruvananthapuram, affiliated to the University of Kerala, Thiruvananthapuram, Kerala, India. She completed her master of science (MSc) degree with a specialization in physics in 2018 from Mar Ivanios College, Thiruvananthapuram (Affiliated to University of Kerala), Kerala, India. She also obtained a master of philosophy (MPhil) in physics (University First Rank Holder) from the Noorul Islam Centre for Higher Education, Tamil Nadu, India, in 2020. She has published more than 35 research publications with an h-index of 17. Her current research focuses on the development of new-generation two-dimensional layered materials, like transition metal chalcogenides and their applications in electrochemical energy storage devices such as rechargeable batteries and supercapacitors. She is a reviewer of several top listed peer-reviewed journals such as Journal of Energy Storage, Journal of Alloys and Compounds, ACS Applied Energy Materials, etc.

Jayesh Cherusseri

Jayesh Cherusseri completed his master's degree (MSc) in physics, followed by a master's degree (MTech) in nanomedical sciences. He obtained a PhD with a distinction in materials science from the Indian Institute of Technology (IIT) Kanpur, India, in 2017. He was a recipient of Dr D. S. Kothari post-doctoral fellowship from India in 2017 and the University of Central Florida (UCF) post-doctoral fellowship in 2018. He has published more than 80 research publications to date with an h-index of 30 with an i10-index of 56, having more than 3000 citations. He has two Indian and one US patent to his credit. He was a recipient of the prestigious Brainpool Fellowship from NRF South Korea in 2024. Dr Cherusseri is currently working as a Brainpool Fellow at Gyeongsang National University, Jinju, South Korea. He was listed in the Stanford University/Elsevier's List of Top 2% Scientists in the World. He is a reviewer of several top-listed journals in the world, such as Nature Communications, ACS Nano, Progress in Materials Science, and Journal of Energy Chemistry. His current research focuses on the synthesis and electrochemical applications of new-generation ultrathin materials.

and future. Herein, we review the recent developments of a biomass material, loofah sponge, for water desalination applications by serving it as a sustainable membrane. Loofah sponge-based materials are highly promising candidates for saltwater desalination. Initially we discuss the salient features of loofah sponge that make it suitable for water desalination applications including chemical properties and further we discuss the synthesis of various natural carbon derivatives from it including mesoporous carbons and biochar. Furthermore, the preparations of composites with other materials systems such as transition metal oxides and MXenes are outlined by emphasizing the microstructural and morphological influence on the performance of membranes for water desalination applications. The present review provides an in-depth understanding of natural loofah sponge-based membranes for desalination application.

Sustainability spotlight

Wastewater purification is mandatory for current and future drinking water standards. Loofah sponge is an environment-friendly sustainable material, which is of low cost and its production is scalable, attracting great interest in the field of wastewater purification. The increasing demand for sustainable water purification technologies is manifested by UN Sustainable Development Goal 6: Clean Water and Sanitation. Accordingly, loofah sponge-based hybrid/nanocomposite membranes are highly sustainable materials for developing wastewater purification by means of membranes for water desalination applications without making any harmful byproducts and pollution.

1. Introduction

Earth's surface is covered with almost 70% of water, but only 2.7% is available as freshwater, and out of which only 0.3% is available as freshwater for human needs.[1,2] With respect to the developments in the field of world economy, growth in population and freshwater resource consumption, the mean value of global per capita freshwater resource has dropped by 50% in the past 50 years. From reports, it is found that three-quarters of the world population will be affected by the shortage in freshwater by 2050.[3,4] After the COVID-19 disaster, pollution in freshwater sources has become a serious problem which accelerated research focus to freshwater resource protection as well as developing novel technologies to convert wastewater to freshwater. This has ended with a number of water treatment technologies being evolved, among which most of them use membranes for the water treatment during the conversion process, such as in the desalination process.[5–7]

Water and energy are the two essential components which are required for human life on Earth.[8–12] Energy scarcity is becoming a nightmare to the world due to the rapid population explosion.[13–17] Scarcity of water is a global issue in the aspect of environmental pollution and human intervention. Both of these issues are somewhat related and influence the overall development in the economic and social context. Desalination is an efficient water treatment technology which generates freshwater by the removal of salt and other minerals and has become a sustainable solution for water treatment and drinking water production globally.[18–22] About 19 000 desalination plants are working to date, which produce almost 1×10^8 m^3 per day of freshwater.[23] Desalination technology is classified with respect to the driving mode of energy required for desalination, namely thermally driven, electrically driven and mechanically driven desalination methods.[24,25] The thermally driven desalination method includes multiple effect desalination and multi-stage flash processes.[26] Mechanically driven desalination refers to a membrane process such as reverse osmosis. Reverse osmosis is a widely used method due to its reduced energy consumption and flexible installation capacity.[27,28] An electrically driven desalination process allows the passage of various ions to pass through a selective exchange membrane under a direct current electric field to produce freshwater. Irrespective of the high energy consumption for these processes, the desalination capacity continues to be increased by about 7% per annum globally.[29] In addition to this, the emerging desalination technology such as the solar water desalination process that combines thermal energy and evaporation of freshwater thereby separating the freshwater, is a feasible and cost-effective method when compared to desalination technologies utilizing electricity. Research and development of solar water desalination are still in their infancy.

With respect to the efficacy in clean water production, solar-driven interfacial desalination is developed as a promising approach with minimization of the carbon footprint.[30–34] Efforts

Deepthi N. Rajendran

Deepthi N. Rajendran completed her master's degree (MSc) in physics, followed by master of philosophy in physics from University of Kerala, Thiruvananthapuram, Kerala, India. She obtained her PhD in physics from the University of Kerala, India, in 2007. She has published more than 60 research publications to date. Her current research focuses on the development of nanomaterials for energy applications, especially in solid oxide fuel cells and supercapacitors. Dr. Deepthi is currently working as an associate professor and research guide at the Department of Physics, Government College for Women, Thiruvananthapuram, Kerala, India. Seven PhDs were produced under her guidance and five students are presently pursuing PhD under her supervision.

have been put forwarded to improve the efficiency of the solar-driven interfacial desalination process, which include optimization in optical absorption, limitation of heat loss and improvement in water evaporation.[35] Salt ions accumulating and crystallising at the evaporator's surface, microchannel clogging, *etc.* weaken the performance of desalination.[36] To address this, salt mitigation strategies such as cleaning salt crystallisation, usage of Janus membranes, and introduction of diffusion backflow replenishment of salt ions through large-sized channels are implemented.[37] A high evaporation rate as well as an efficient salt resistance are difficult to attain simultaneously when using concentrated brine water during a long evaporation process.[38] For a sustainable future, it is necessary to develop renewable and sustainable water purification technologies that should be cost-effective and environmentally friendly. In this context, solar water desalination is a promising method, which is considered to be a green technology.[39] The cost effectiveness, availability, and sustainable character make the solar evaporation technique a promising route for purifying wastewater, desalination of seawater, and steam disinfection. In comparison with the traditional water purification methods, solar desalination exhibits higher thermal efficiency, reduced maintenance cost, flexibility, and ability to control the production cost.[40] In the solar desalination process, the water gets converted to steam at the interface of air and water hence the interfacial evaporator material plays a crucial role in absorbing the heat and its passage. The heat absorbed by the evaporator is dissipated in the form of conduction, convection, and radiation.[41] Various types of materials are used to prepare the solar interfacial steam generators with a two-dimensional porous architecture being proposed. In general, a two-dimensional evaporator has three components: a solar absorption layer having high light absorptivity, a conveyance water structure having porosity and high hydrophilicity, and an insulating substrate with a reduced thermal conductivity. With respect to the deepening strategy for the solar absorption layer features and substrates, an increase in the number of materials and layer structures has been used.[42] Currently, a solar absorption layer is made of metal particles of plasma, semiconductor, and carbon components. These materials allow conversion of solar energy to heat energy by obeying the principles corresponding to local heating of plasma, creation and relaxation in electrons, holes, and molecular thermal vibration.[43] Among the various available choices, carbon materials possess features such as broadband absorption and good photothermal features, which are broadly investigated. Although carbon-based photothermal systems are developed, some of the scientific problems still need to be resolved. Nanostructured carbon materials such as carbon nanotubes, graphene, graphene oxide, *etc.* are widely used as photothermal absorbing materials for desalination applications.[44–48] The major drawback of using these materials for commercial applications lies in their huge cost associated with their synthesis; hence their applications are limited.[30,49,50] To address this issue, biomass-derived carbon materials are chosen and are found to be effective materials which maintain their structure and morphology after carbonization.[51] In comparison with synthetic materials, biomass-based materials have less negative impact on the environment. Presently, the major biomass materials explored include bamboo tree, wood, pollen, mushroom, algae, *etc.*[52–54] The evaporation rate of a wooden evaporator is a lower value of about 0.5–1.17 kg m^{-2} h^{-1}.[55] Mushroom, biomass, and other carbon components have the ability to retain their structure after carbonization. But the major demerit is their high cultivation cost and longer duration required for cultivation. For example, in the case of mushroom it takes about 4 months and for bamboo, it takes about 1 year. In addition to this, when biochar materials are applied in interfacial evaporation, they cannot be perfectly sliced and arranged to create a large-area evaporation because their own structure is not in a flat form. After performing carbonization, smaller particle structures like algae and pollen couldn't be used for interfacial evaporation directly without using binders. These binder materials are water-insoluble and need to be dissolved in organic solvents like *N*,*N*-dimethylformamide to prepare films, which leads to high production costs as well as water pollution. Thus, it is urgent to develop new materials which are easy to prepare without using binders so that the evaporator will be green, efficient, and afford pollution-free evaporation. By taking into account these facts, material researchers and water scientists are highly dedicated to developing other evaporators that are free from drawbacks when compared with other materials. Naturally occurring plants like mangroves thrive in water with salinity greater than that of seawater. Generally, mangrove root layer has high surface ζ-potential of approximately −91.4 ± 0.93 mV. With inspiration from the mangrove root layer which is negatively charged, a polyelectrolyte hydrogel is used with respect to its unique salt-rejection effect for high charge, this

Fig. 1 Contents of the present review. (a) Digital photograph of dried loofah sponge. Reproduced with permission from ref. 58. Copyright (2023) Elsevier Inc. (b) Cross-sectional SEM image of inner side of loofah fiber. Reproduced with permission from ref. 58. Copyright (2023) Elsevier Inc. (c) Digital photo of an outdoor water desalination setup. Reproduced with permission from ref. 58. Copyright (2023) Elsevier Inc. (d) Loofah sponge biochar evaporator. Reproduced with permission from ref. 42. Copyright (2022) Elsevier Inc. (e) Digital image of loofah plant. Reproduced with permission from ref. 61. Copyright (2020) Royal Society of Chemistry.

being termed a mangrove root with similar manner in the desalination of water. Despite a polyelectrolyte hydrogel network, indigenous design of an evaporation configuration to increase dynamic water transportation is another parameter to optimize the efficiency of solar desalination. In this review article, we describe the salient features of a biomass material, loofah sponge, for application in water desalination applications. Loofah sponge is a highly promising biomass material, which is a naturally occurring plant fiber. We discuss its importance in water desalination applications including the synthesis of absorber materials, their properties, and performance evaluations. The content of the present review is schematically shown in Fig. 1.

2. Features of loofah sponge

Loofah sponge is commonly named as a vegetable sponge, which is obtained from the mature dry fruit of *Luffa cylindrica*. It is composed of crisscrossed fibers and includes a three-dimensional (3D) reticular architecture. Photographs of raw *Luffa cylindrica* and dried loofah sponge are shown in Fig. 2(a–c).

The loofah sponge is a rich plant resource and it is commonly cultivated in tropical countries of Asia, Africa and other sub-tropical regions. The attractive features of loofah sponge include reduced density, eco-friendliness, non-toxicity, biodegradability, and low cost. There exist two types of loofah sponges: one with high density and the other with low density. There are many varieties of the former. Applications of these loofah sponge materials were studied widely in China, almost 400 years ago. The Chinese classic "*Compendium of Materia Medica*" recorded the performance of loofah sponge and indicated that "loofah sponge, with sweet and clod nature, has the effect of clearing heat, cooling blood, detoxifying, promoting circulation of blood and dredging collaterals". Loofah sponges

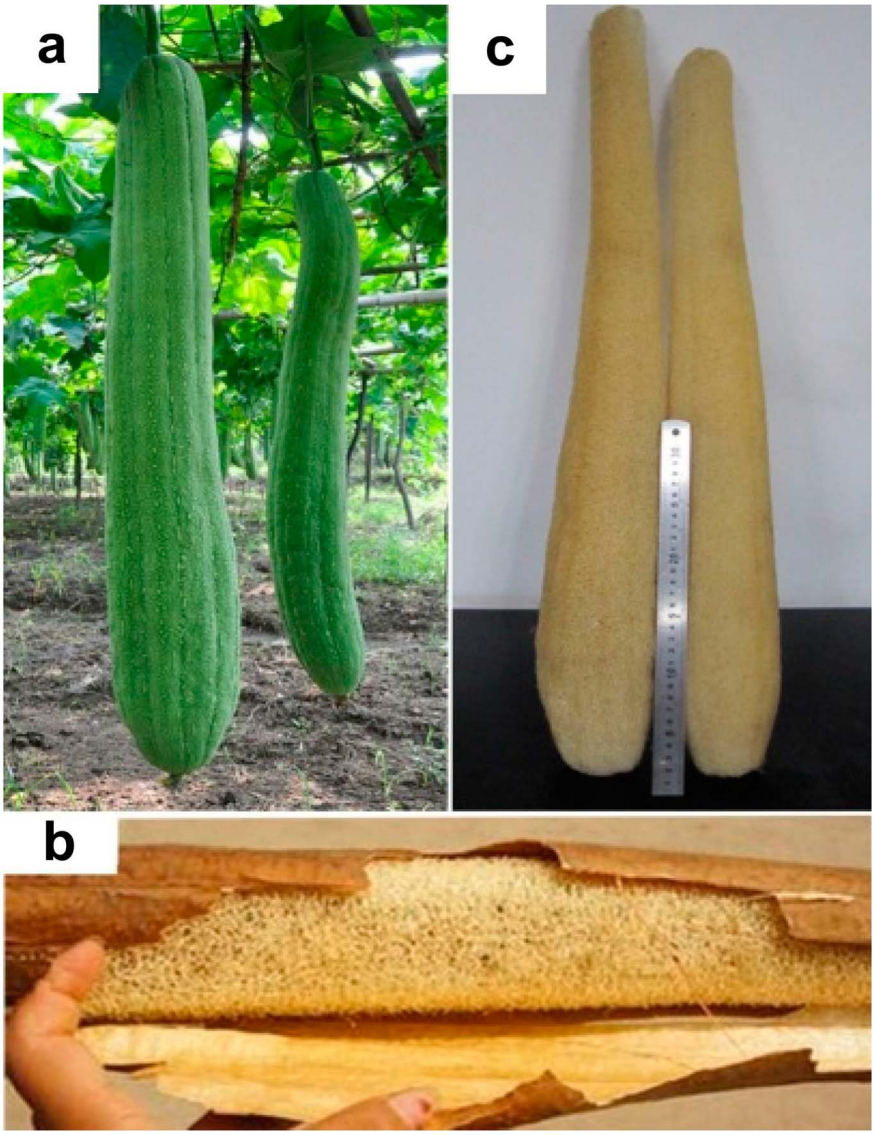

Fig. 2 Digital photographs of (a) cylindrical loofah, (b) cortex in loofah sponge, and (c) loofah sponge. Reproduced with permission from ref. 56. Copyright (2017) MDPI.

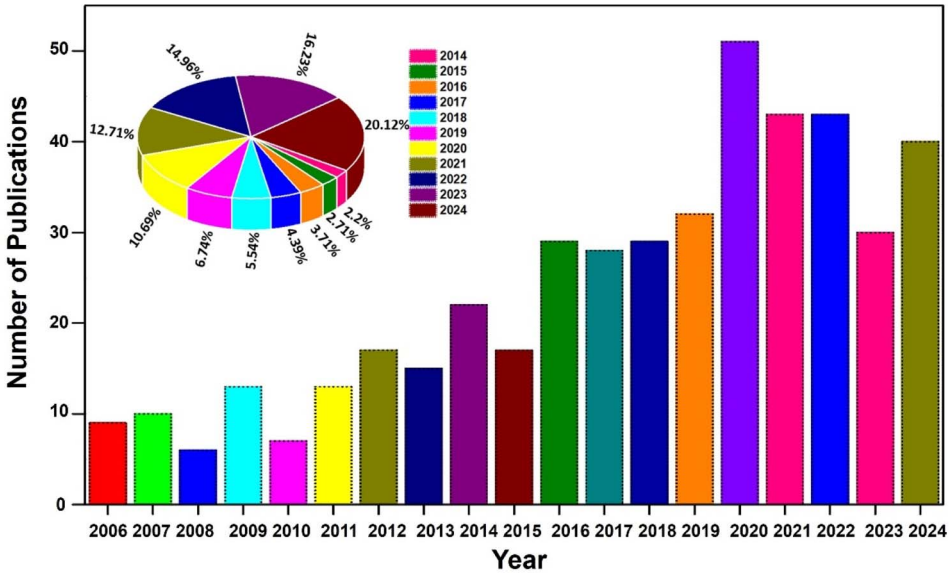

Fig. 3 Statistical representation of the number of publications based on loofah sponge for various applications during 2006–2024. The inset represents the percentage of citations received for these publications [source: Web of Science].

are used for cleaning devices, pillow filling and insole material. Advancements in science and technology have led to the application of loofah sponge in several fields of environmental engineering, pharmaceutical engineering, industrial engineering, and biomaterials science. With respect to the highly porous character, biochar materials are prepared from loofah sponge that can be further used in adsorption, electromagnetic interference shielding, *etc.* The porous nature of loofah sponges is associated with a higher degree of lignification, and it is a promising biomass material for a variety of applications.[56]

Loofah sponge is largely available as a dried sponge, which is a cost-effective biomass introduced from loofah plant fruit and a commonly used cleaning tool with light-weight nature. Loofah sponge is a cheap and widely available biomass having useful mechanical strength and dimensional stability that has a hydrophilic nature and hemicellulose favouring the absorption and transfer of water. It possesses a 3D network that acts as a self-supporting substrate with porous architecture facilitating enough space for air flow and ion exchange. By considering the features of loofah sponge and loofah sponge-derived materials for desalination, material researchers and water scientists are currently exploring these materials as efficient candidates for desalination applications. Among the various reports, some of them are dedicated to the use of loofah sponge in water purification whereas others are focused on the application of loofah sponge in the desalination treatment of salt water to produce

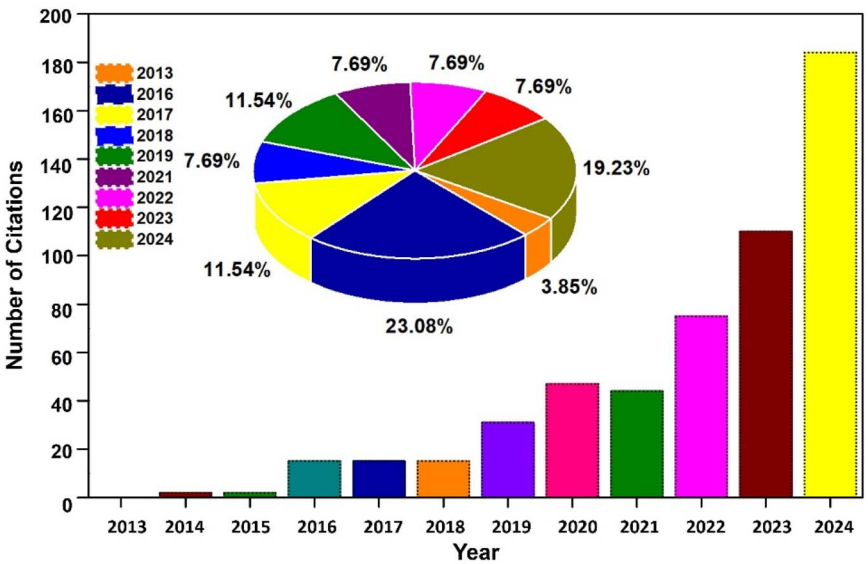

Fig. 4 Statistical representation of the number of citations received for the publications based on loofah sponge for water purification during 2013–2024. The inset represents the percentage of number of these publications [source: Web of Science].

pure water. A statistical representation of the number of publications based on loofah sponge for various applications for the calendar years 2006–2024 is shown in Fig. 3. The percentage of citations obtained for these publications during the period 2014–2024 is given as an inset image in Fig. 3.

From this figure, it is clear that there is an increasing research interest in using natural loofah sponge for a variety of applications. Although the application of loofah sponge is reported in 2006, its application in water purification is firstly reported in the year 2013. The number of citations received for the loofah sponge-based publications for water purification for the calendar years 2013–2024 is shown in Fig. 4 and the number of publications (in %) in each year is given as an inset image. A review in the field of loofah sponge-based clean water production is not reported in the literature and hence it is mandatory and timely to understand the salient features of this material as well as the preparation of loofah sponge-based materials for water desalination performance enhancement.

3. Loofah sponge: an effective material for desalination

Loofah sponge biochar is a potential material to develop a solar absorption layer and its low cost and short cultivation cycle of 2–3 months have attracted research interest.[57] The processing of loofah sponge avoids any complex approaches like molding and binder preparation for the synthesis. It is possible to utilize its structure directly as a solar absorption layer for an interfacial evaporator after performing pressurization and carbonization in a simple way without any addition of extra reagents. Network architecture of these loofah sponges is prominent in splicing, which produces a large areal evaporation. Loofah-based polyelectrolyte hydrogel evaporator having bilayer structure is designed to meet higher evaporation characteristics to introduce highly efficient desalination for long-term performance.[58] A design of bilayer polyelectrolyte hydrogel with loofah sponge was developed to meet the higher performance requirement for water desalination. By mimicking the root layer of mangroves with negatively charge as shown in Fig. 5a, sodium polyacrylate carbonized loofah is prepared with a carbonized top layer and coated with a polyacrylate hydrogel on the network to induce salt resistance. The top portion of the carbonized layer has broad light absorption and efficient light capturing, which acts as solar absorber. But in the microchannels, restricted counter ions, Na^+ ions, produce a Donnan potential, tending to redistribute nearby in brine solution, leading to a salt resistance effect. At the same time, a unique hydrophilic hierarchical channel in loofah efficiently manages the water content in solar steam generation. Sodium polyacrylate carbonized loofah

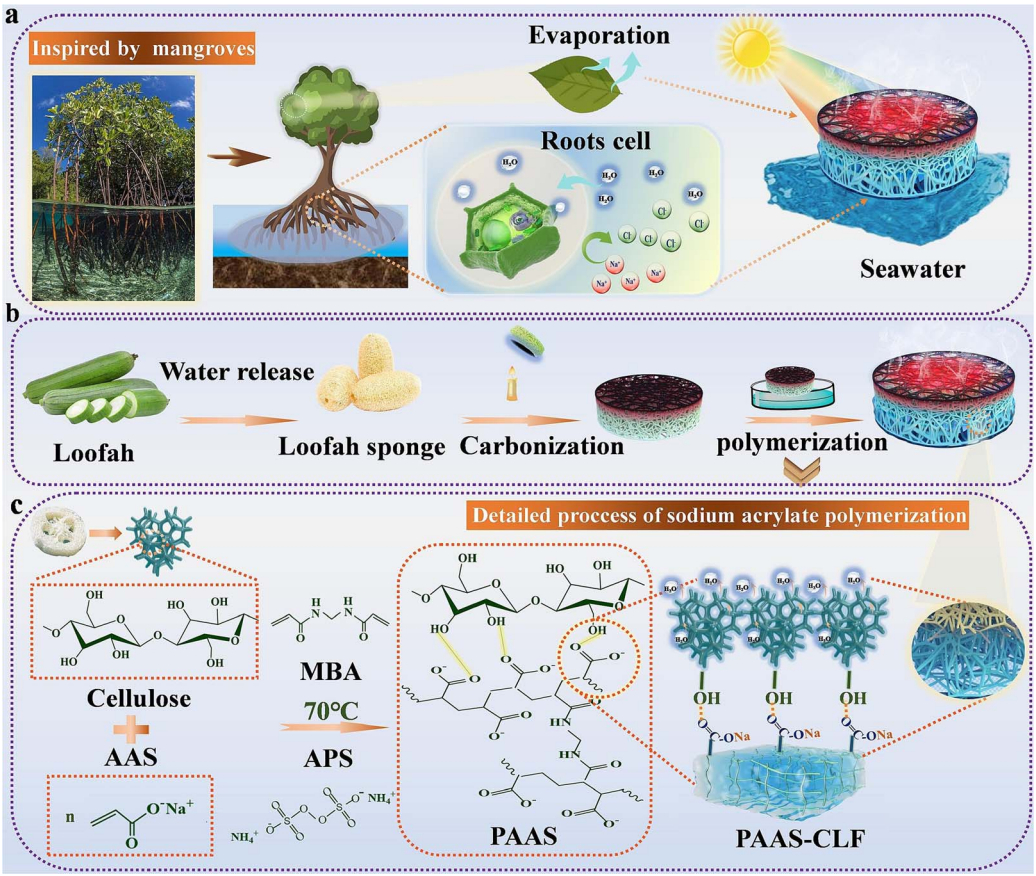

Fig. 5 (a) Generation of mangrove-inspired solar vaporization; (b) synthesis process in sodium polyacrylate carbonized loofah; (c) detailed procedure of polymerization of sodium acrylate on loofah. Reproduced with permission from ref. 58. Copyright (2023) Elsevier Inc.

bilayer structure consists of two parts: a carbonized top layer and a sodium polyacrylate hydrogel embedded in a microporous layer at the bottom with carbon loofah fiber for the supply of water. Loofah fiber is chosen as a substrate because of its reduced cost, effective hydrophilicity and the occurrence of microporous channels in it. The preparation of this proposed loofah fiber is shown in Fig. 5b. Initially, the top surface layer of loofah sponge is carbonized to increase the absorption of light. Later, sodium polyacrylate is synthesized by *in situ* polymerization of acrylic acid present in the network, which leads to highly efficient water retention and ability for salt resistance to allow solar desalination. Polymerization procedure for the sodium polyacrylate hydrogel is given in Fig. 5c. Loofah bottom layer is then submerged in sodium acrylic acid solution to ensure solution fills its pores and kept in an oven for copolymerization. The large number of hydroxyl groups in cellulose of the loofah skeleton and carboxyl groups present in sodium polyacrylate help in cross-linking the polymer chains by non-covalent hydrogen bonding.

The morphological and structural evaluation of loofah fiber and sodium polyacrylate carbonized loofah is shown in Fig. 6. Loofah harvested in the early stage is an edible component, but a fully matured loofah act as a fibrous material (Fig. 6a). A scanning electron microscope (SEM) image of loofah with the corresponding energy-dispersive X-ray spectroscopy (EDS) mapping images are presented in Fig. 6b. The SEM image elucidates that the structure has microchannels in loofah fiber, mostly lying in the micropore range for the transportation of water and a steam channel pathway inside. Fig. 6c shows the FTIR spectra of loofah fiber. EDS spectra of sodium polyacrylate confirming the distribution of elements C, O and Na suggest the homogenous modification of surface of loofah by sodium polyacrylate. The characteristic peaks originate from the sodium polyacrylate in the corresponding carbonized loofah fiber. The natural layer untreated exhibits a porous interconnected structure that could hold hydrophilic loofah cellulose fibers (Fig. 6d). Fig. 6e and f present cross-sectional SEM images at two different magnifications show continuous arrangement of a honeycomb structured microchannel and its diameter is in the range of 15 μm. The original shape of loofah is found to be retained even after undergoing carbonization. An illustration of a macropore coated with sodium polyacrylate carbonized hydrogel after performing the copolymerization procedure is shown in Fig. 6g, which indicates an efficient synthesis of loofah fiber-based sodium polyacrylate carbonized hydrogel. The SEM images show the sectional loofah fiber (Fig. 6h and i) which is smooth as a result of sodium polyacrylate carbonized hydrogel polymerization to attain higher evaporation rate of water without making any change in its inherent structure of multiple microchannels inside the fibers. In addition to this, it is found that the hydrogel-coated loofah fiber exhibited a high porosity of about 96.54% after the coating process.

A solar desalination experiment was performed with carbon loofah fiber and four evaporators having various contents of sodium polyacrylate hydrogel carbon loofah fiber kept in seawater under 1 sun. The authors of this work observed that

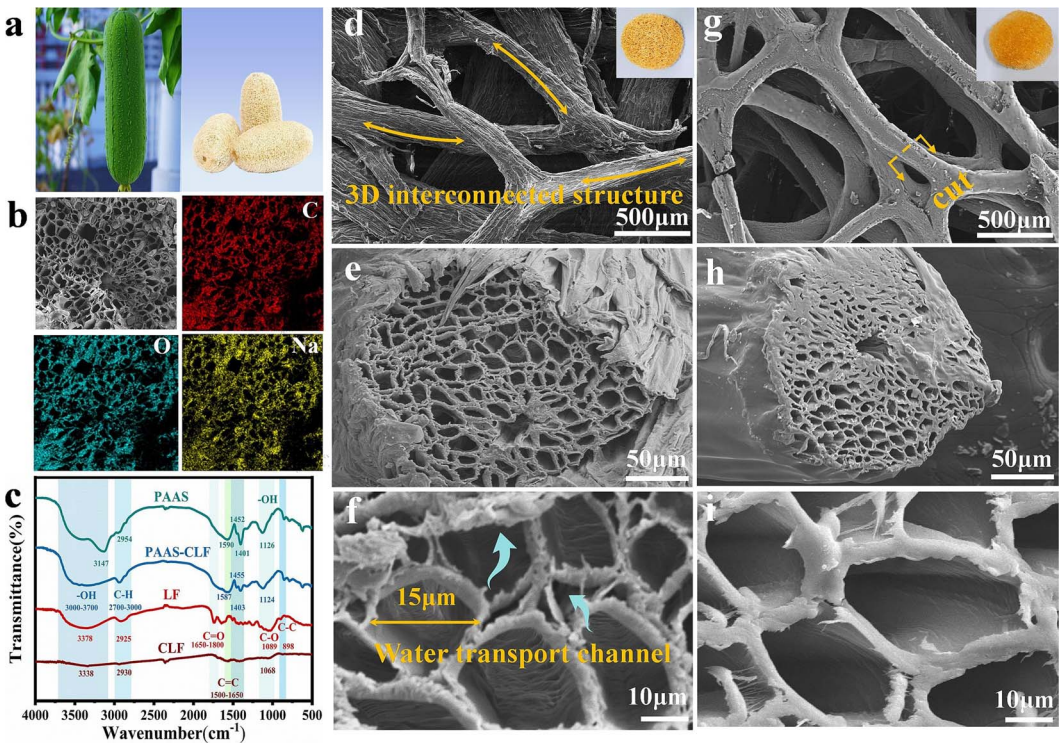

Fig. 6 (a) Loofah fiber photograph; (b) SEM image of loofah sponge and corresponding EDS mapping; (c) FTIR spectra; (d) 3D porous structure in loofah fiber; (e and f) cross-sectional views inside loofah fiber; (g–i) surface and sectional SEM images of sodium polyacrylate carbonized loofah. Reproduced with permission from ref. 58. Copyright (2023) Elsevier Inc.

carbon loofah fiber exhibited a reduced salt rejection value of 8.6%, indicating that there exists a large quantity of NaCl growth inside the hydrogel. This salt rejection value of sodium polyacrylate hydrogel-carbon loofah fiber is found to be increased with respect to the concentration of sodium polyacrylate loading amount and it is found to be 60.1%, 73.4%, 80.2%, and 82.4% for 10, 15, 20, and 25 wt%, respectively. By evaluating the repeatability character of sodium polyacrylate carbon loofah fiber for ten cycles, a stable performance was obtained, although there was an accumulation of salt on the surface. The assembled evaporator maintained a salinity from 36 to 200 g kg^{-1} without any deposition of salt for longer time of desalination. The practical applicability of outdoor solar desalination was also evaluated by the authors of this work. A schematic representation and construction pattern of solar water purification with solar energy are shown in Fig. 7a and b, respectively. The production of water vapour with sodium polyacrylate carbon loofah fiber on the left contacts the glass plate and forms into water droplets by collecting in the right chamber. This sodium polyacrylate carbon loofah fiber not only introduces clean water for desalination but it also exhibits excellent performance in water remediation that removes metal ions, organic dye, alkaline and acidic solutions in sewage, as depicted in Fig. 7c. The pH measured for acidic and alkaline solutions in sewage before and after the desalination are depicted in Fig. 7e. Further, the concentrations of four cations (Na^+, Ca^{2+}, Mg^{2+}, and K^+) in the purified water were determined after the desalination process and found to be lower than those suggested by the World Health Organization (WHO) as shown in Fig. 7d and the test results for the other four cations are depicted in Fig. 7f.

Activated carbon synthesized from the loofah sponge using phosphoric acid was used for adsorbing cefalexin present in aqueous solution.[59] The activated carbon exhibits a porous architecture having micropores and mesopores and shows 95% adsorption for cefalexin. It exhibits maximum adsorption efficiency of 55.11 mg g^{-1} at a temperature of 308 K. The authors of this work observed that the equilibrium data agree with the Freundlich isotherm, which represents multilayer adsorption and cefalexin adsorption by activated carbon, indicating a pseudo-second-order reaction. It is possible to use an aminated phenolated lignin by combining with hydrophilic polyethylene glycol onto hydrophilic loofah sponge.[60] The authors of this work introduced lignin as a material for photothermal conversion and it shows an efficient and a controllable efficiency for photothermal conversion through adjusting the amount of grafted conjugated structures in a simple procedure. The authors introduced lignin as photothermal conversion

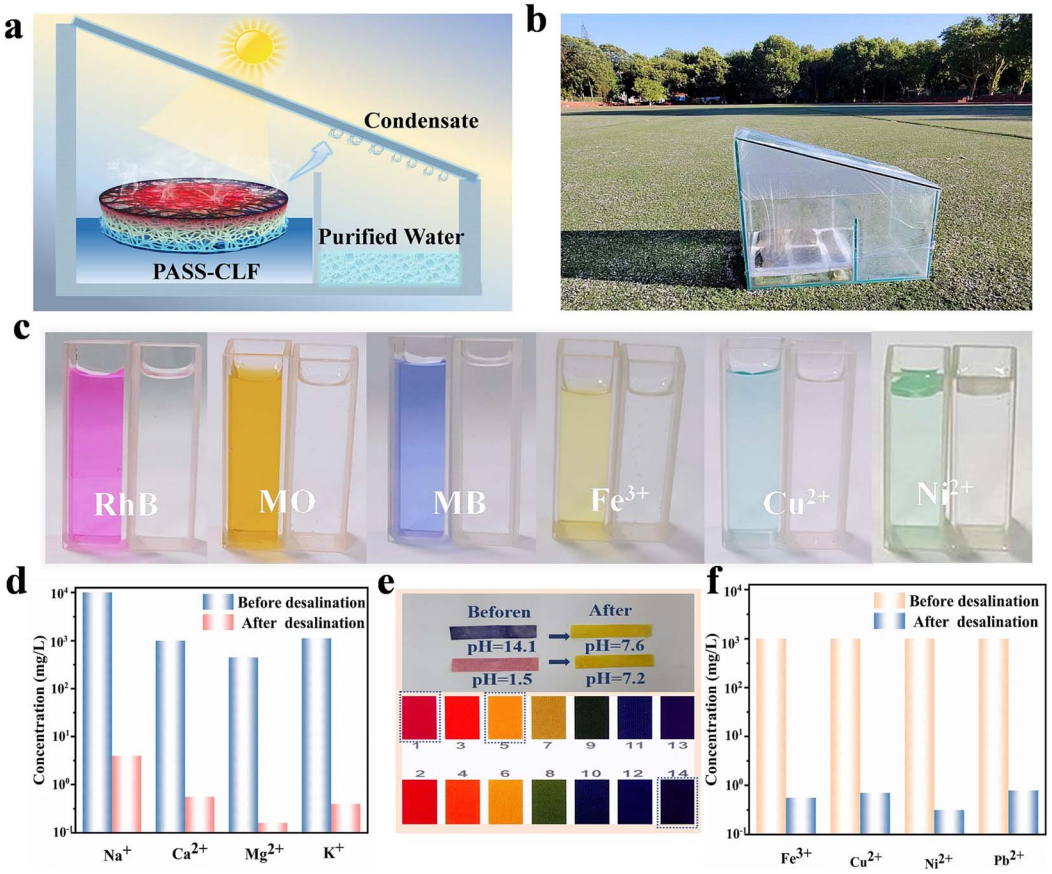

Fig. 7 (a) Pictorial representation and (b) digital photo of an outdoor setup; (c) heavy metal ion and dye before and after purification; (d) primary element concentration in saltwater before and after performing desalination; (e) pH value measured for acidic and alkaline solutions in sewage; (f) heavy metal ion concentration after performing purification. Reproduced with permission from ref. 58. Copyright (2023) Elsevier Inc.

candidate for solar evaporator fabrication because of its strong and efficient π–π molecular interaction. An evaporation efficiency of 97.6% with an evaporation rate of 1.75 kg m^{-2} h^{-1} is achieved under 1 sun illumination. A bilayer structure of loofah sponge was developed, which consists of a blackened top layer and a native alignment of the bottom layer having good light and water absorption characteristics for a stable and sustainable solar evaporator. For the top layer, the black-coloured rough loofah fiber surface exhibits an antireflection performance. At the same time, light is trapped between the layered porous mesh. An image of a loofah fruit is shown in Fig. 8a. There exists a limitation in the broad solar absorption spectrum of native loofah sponge. To optimize the solar-driven evaporation application of loofah sponge, a carbonization procedure was performed to blacken the surface layer. This leads to a dramatic increase in absorption of light at the top layer, which is schematically shown in Fig. 8b. In comparison with a non-integrated double-layered structure, the proposed integrated bilayer architecture in this work removes the gap between two layers for minimizing the thermal and water resistance. The evaporator thus fabricated showed an integrated architecture having a carbonized layer of thickness ~2 mm on the top surface to facilitate adsorption of light. In addition to this, there is an untreated natural layer having thickness ~8 mm in the bottom of the evaporator. The light absorption occured at the solar evaporator is schematically shown in Fig. 8c–e. In comparison with a flat and dense structure, the interconnected porous architecture consists of coarse fibers which thereby increases absorption of light by trapping, increase in surface area, and antireflection phenomena. There are three major

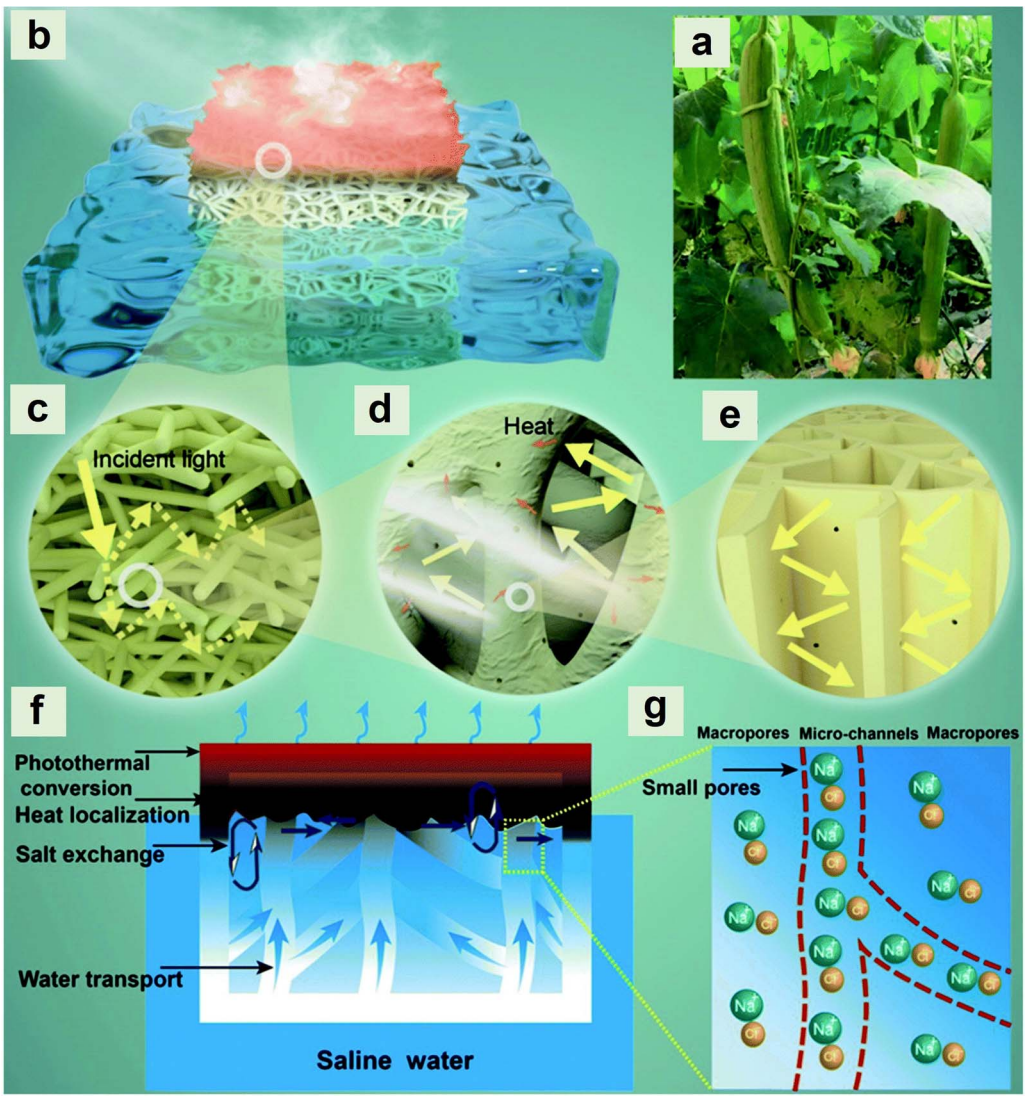

Fig. 8 (a) Digital image of loofah plant. (b) Schematic representation of loofah sponge-based solar steam introduction system prepared on a large scale with surface carbonized loofah sponge. (c) Multilayer architecture of evaporator. (d) Macropore of evaporator. (e) Microchannel of evaporator. Mechanism corresponding to transfer of mass in evaporator. (f) Evaporator has several features like vapor transportation of interconnected microchannels, broader spectrum of absorption of light in carbonized surface as well as properties of heat localization and interfacial salt exchange. (g) Concentration of salt gradient between microchannel and macropore enabled exchange of salt for preventing this salt accumulation. Reproduced with permission from ref. 61. Copyright (2020) Royal Society of Chemistry.

phenomena for this trapping of light. The first one is the internal light scattering and trapping in this multilayer structure having limited availability of space between the layers (as shown in Fig. 8c). Secondly, the light makes multiple reflections inside macropores introduced between fibers (Fig. 8d). Thirdly, it is clear from Fig. 8e that microchannels present inside the fiber maximize light absorption with trapping of light inside channels. On the other hand, hydrophilic loofah cellulose fiber having abundant hydroxyl groups can make a quick absorption of water. Besides this, hydrophilicity and microchannel combination make the surface of infiltrating liquid as a capillary, producing a rising of liquid along the microchannel wall. Here, the hydrophilic fiber and its internal microchannel structure provides enough water supply for the transportation of water to heat the surface by capillary action (Fig. 8f). When the water absorbed in the localized heat surface evaporates, it introduces tension; hence it becomes difficult to balance and maintain running cycles. Moreover, water transfers from different directions to localized surface heating through pores connected at the microscale. During the process of desalination, evaporation of water continuously on the upper surface leads to an increase in concentration of salt at the localized heating surface. From Fig. 8g, we can find that salt concentration in microchannels is much higher than that of macropores in sponge due to the limitation in water content of microchannels, producing a horizontal salt concentration gradient. Here, the distribution of salt concentration is in the order of upper-layer microchannel > upper-layer macropore > lower-layer microchannel > lower-layer macropore. The concentration gradient of salt leads to a salt exchange between microchannels and 3D porous structure in sponge. In the vertical direction, there exists a spontaneous exchange of highly saline water in the upper layer with lower saline water in the lower layer for diluting the concentration of salt in the upper layer (Fig. 8f). At the same time, loofah sponge exhibits efficient hydrophilicity which rapidly absorbs the water to vaporize brine at the heating surface to remove accumulation of salt. The inherently present porous architecture in fibers and microchannels addresses the accumulation of salt spontaneously.

A digital image of a native loofah sponge is shown in Fig. 9a. There exists a 3D porous architecture between fibers and different layers which have pores with varied sizes. The surface morphology of loofah sponge is studied further by SEM imaging. From Fig. 9b, it is clear that the evaporator upper layer retains its original shape after carbonization. Here, the upper carbonized layer has an interconnected porous structure, benefiting light transportation. Unlike a flat surface which depends upon the angle of incident light, a coarse fiber cylindrical surface helps in increasing the specific surface area for absorption of light to a greater extent. Here, sunlight absorption was effectively maintained throughout the day. Multilayered architecture extends the multi-scattered optical pathways and causes a reduction in reflectivity, contributing ultra-high light absorption capacity to the evaporator. The macropores introduced in fibers facilitate light trapping. Here, incident light tends to produce multiple reflections inside macropores and microchannels, which increases the light absorption of the material and generates heat. The unique structure of microchannels inside fibers leads to light trapping as shown in Fig. 9c. Zoomed views of the channel structure of the evaporator are shown in Fig. 9d–g. These channels make a continuous arrangement and the channel diameter ranges from 10 to 20 μm. These well-arranged channels make an extension in the coarse fiber direction as shown in Fig. 9f and g. The authors of this work evaluated the solar-driven evaporation capability of the loofah evaporator with respect to the mass change of water in a beaker under different solar irradiation powers of 1, 2, 3, and 5 sun at 20 °C with 40% humidity. At the same time, by the optimization of the carbonized layer of the evaporator having various thicknesses, a higher performance was obtained for a layer thickness of 2 mm. During evaporation, water evaporates in the form of steam over the loofah-based evaporator, as shown in Fig. 10a. A pictorial representation of a solar-driven steam generator is shown in Fig. 10b. Here, the evaporator is placed in a container that is floated on water, without any of the auxiliary equipment. A perfect balancing of the combination of broadband adsorption of light, localization of heat, water evaporation, and water supply facilitates a higher evaporation rate and efficiency of conversion. The mass change of pure water, natural loofah sponge, carbonized wood, and carbonized loofah sponge under illumination of 1 sun is shown in Fig. 10c. In accordance with this 3D porous architecture, the microchannel behaves as a capillary in fibers of loofah sponge, having an evaporation rate of 1.42 kg m^{-2} h^{-1}, which is greater than that of natural loofah sponge (0.45 kg m^{-2} h^{-1}) or a wood evaporator (0.82 kg m^{-2} h^{-1}). Natural loofah sponge exhibits a lower value for solar absorption because of the lack of natural colour and unidirectionally aligned wood channels. This interconnected microchannel provides water absorption which transports to the surface of the evaporator from different directions, which promotes water evaporation. The authors also determined the rate of pure water evaporation. The evaporation rate shown by this loofah-based evaporator is 6.5 times greater than that for pure water where it was only 0.22 kg m^{-2} h^{-1}.

The evaporation rates shown by this loofah-based evaporator at different solar irradiation powers are depicted in Fig. 10d. The variation in the evaporation rate and the efficiency of carbonized loofah sponge at different optical concentrations are shown in Fig. 10e. An increase in solar illumination power can produce a high evaporation rate and reached a maximum evaporation rate of 6.62 kg m^{-2} h^{-1} under 5 sun. The efficiency of carbonized loofah sponge is found to be 89.9%, 92.0%, 90.1%, and 90.7% for 1, 2, 3, and 5 sun, respectively. The cyclic performance of the evaporator at different solar illuminations of 1, 2, 3, and 5 sun, each cycle being sustained for more than 1 h, is shown in Fig. 10f. Here, the evaporator introduces a superior character for reusability. The authors of this work compared the performance of the carbonized loofah sponge-based solar evaporator with those reported in the literature as depicted in Fig. 10g. From this graph, it is clear that the evaporation rate and efficiency of carbonized loofah sponge are higher than many of the reported works. The advantage of this work is scalability. As it is easy to synthesize loofah sponge membrane by physical and chemical methods in a short

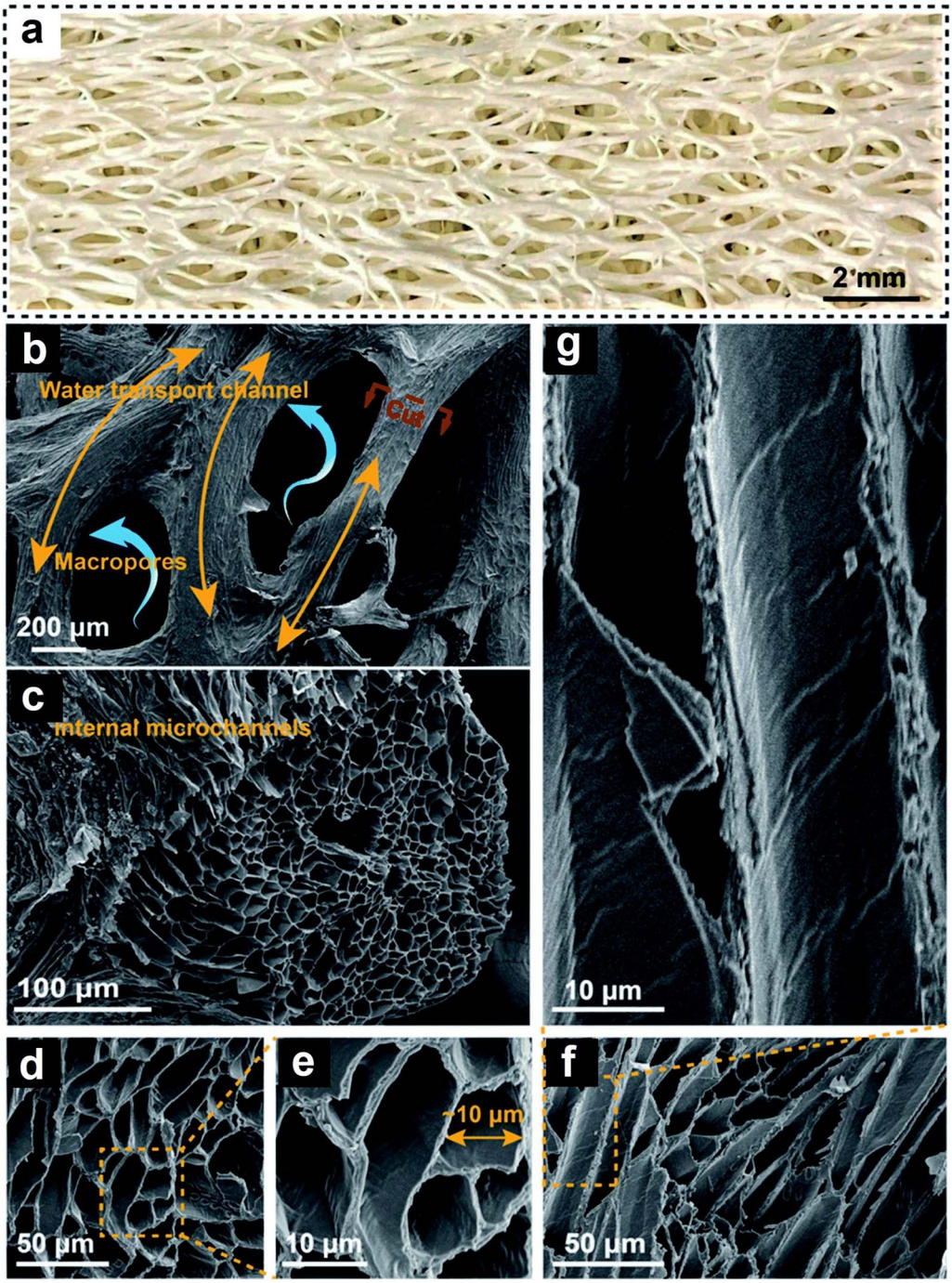

Fig. 9 Structural and morphological characterization of loofah-sponge-based evaporator. (a) Digital image showing geometrical feature in loofah sponge; (b) SEM image of loofah fiber, (c) SEM image representing a cross-sectional view of multiple microchannels inside the fiber; (d and e) SEM images of channel structure at different magnifications; (f and g) along-channel SEM images with interlaced channel at various magnifications. Reproduced with permission from ref. 61. Copyright (2020) Royal Society of Chemistry.

processing time and no sophisticated equipment required. Hence, the production cost is very low, being highly economical for potential marketing and commercialization.

One of the methods available for the synthesis of a loofah sponge-based solar absorption layer in a solar interfacial evaporator is by compression and carbonization.[42] In a typical procedure, loofah sponges are initially prepared by removing the seeds from common towel gourd and then drying. Insulation substrate is synthesized from polystyrene foam with a density of 11 kg m^{-3} and a water transport structure is made from melamine foam having a density of 8 kg m^{-3}. Chemical reagents utilized for the synthesis of the absorption layer are ethanol, potassium chloride, sodium chloride, calcium chloride, magnesium sulfate, sodium bicarbonate, and magnesium

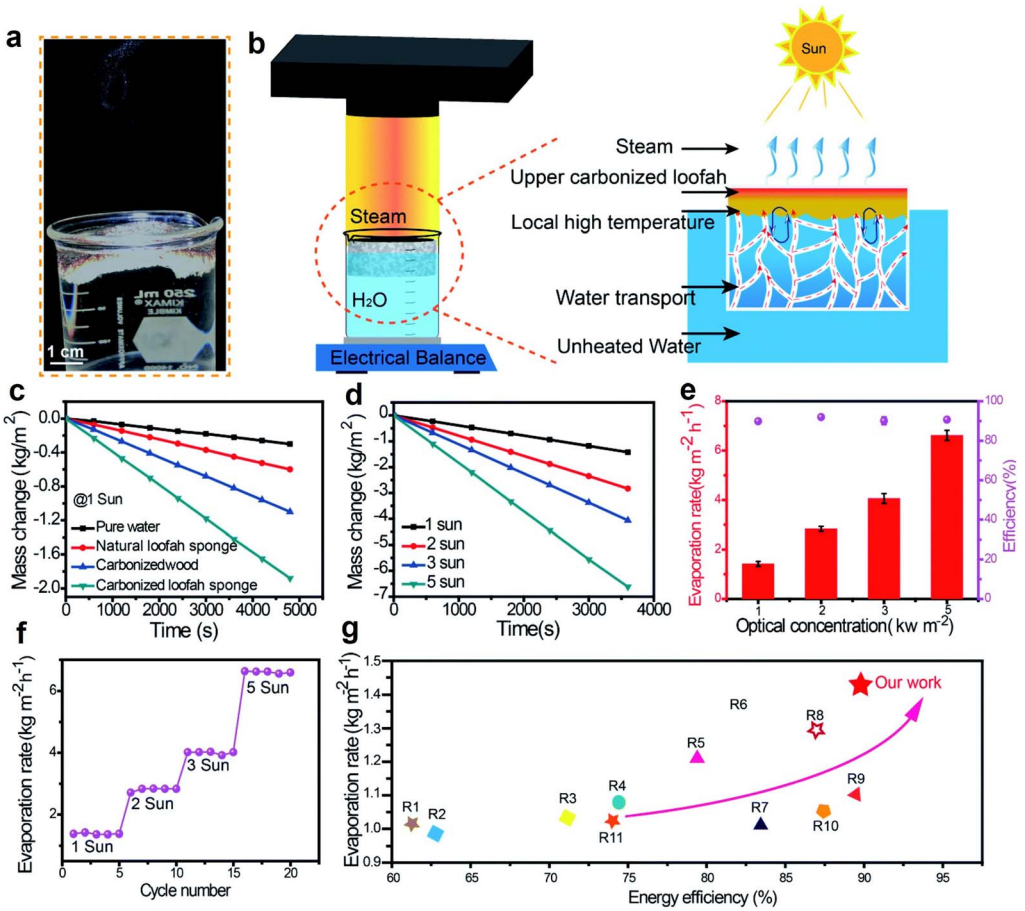

Fig. 10 Loofah-based evaporator setup and its characterization. (a) Digital image of visible vapor created with illumination of 3 sun. (b) Schematic representation of solar water evaporation experimental arrangement. (c) Change in mass of water with pure water, natural loofah sponge, carbonized wood and carbonized loofah sponge with irradiation of 1 sun. (d) Change in mass of carbonized loofah sponge. (e) Evaporation rate and efficiency of carbonized loofah sponge under solar illumination powers of 1, 2, 3, and 5 kW m^{-2}. (f) Water evaporation cyclic characteristics of carbonized loofah sponge with different solar illumination rates, each cycle being sustained for greater than 1 h. (g) Evaporator system production with loofah sponge in comparison with previously reported values under an irradiation of 1 sun. Reproduced with permission from ref. 61. Copyright (2020) Royal Society of Chemistry.

nitrate. Solar absorption layers with two kinds of loofah sponge biochar are shown in Fig. 11a. The synthesis procedure for compressed loofah sponge biochar involves three steps of compression, washing and carbonization. Here, a cylinder of 5 cm in diameter is cut from the outer ring of loofah sponge, which has a thickness in the range of 0.6–0.8 cm. This loofah sponge cylinder is further washed using deionized water and dried in an oven at 50 °C for 2 h. Further, these materials are kept in a tubular furnace for pyrolysis at 800 °C with a heat rate of 2 °C min^{-1} under nitrogen atmosphere for 2 h. Natural loofah sponge has a porous architecture where the pores consist of large gaps between fibrous structure. There exists a diverse structure in these naturally grown loofah sponges. These pores provide efficient channels for water and steam transportation. At 800 °C, loofah sponge lost its water content and shrank, producing pores and biochar structure that is more compact. A schematic representation of structure of internal and external water conveyance substrate is shown in Fig. 11b. Fig. 11c compares the structure of a loofah sponge biochar evaporator. From the SEM images provided in Fig. 12a and b, it is clear that loofah sponge biochar maintained a porous architecture, with a skeleton surface roughness. This biochar is arranged in the form of fiber clusters, which are intertwining with each other and there exist many pores in the fiber surface. From the cross-sectional view of loofah sponge biochar, it is clear that there exist tubular holes in fiber, and the internal diameter of the holes is in the range of 4–10 μm. The pore size of loofah sponge biochar is increased in comparison with natural loofah sponge due to an increase in specific surface area from 1.8 to 544.1 m^2 g^{-1}. The BET N_2 sorption isotherms for these two materials are given in Fig. 12c.

Because of the presence of hemicellulose, cellulose, and other constituents in the loofah sponge, it undergoes a decomposition at high temperature, producing volatile substances like H_2O, CO and CO_2. The evaporation of these volatile substances tends to make towel gourd biochar pores abundant. However, these volatile substances sometimes create a large number of holes during evaporation. On irradiation of sunlight to the

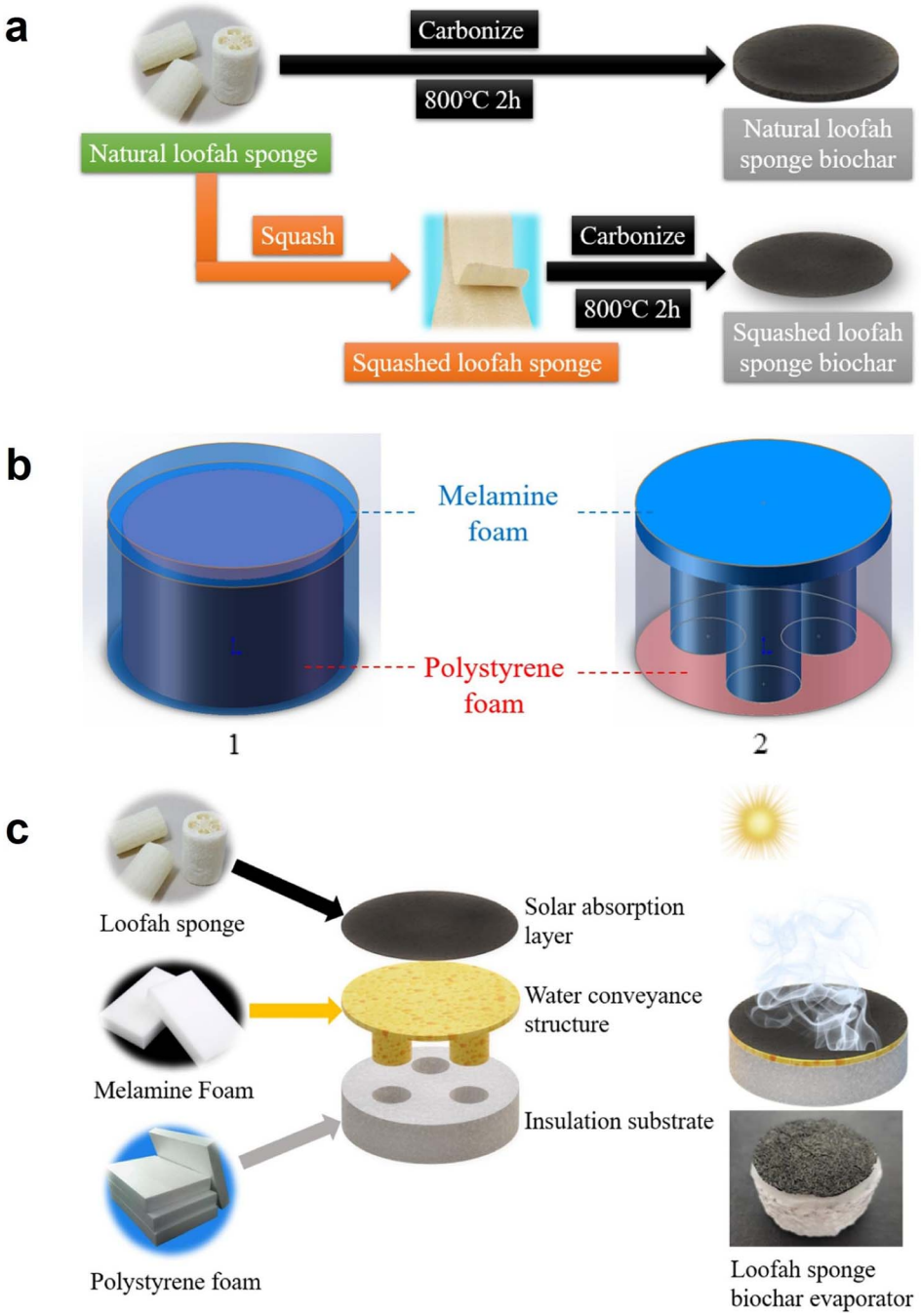

Fig. 11 (a) Synthesis process of loofah sponge biochar solar absorption layer. (b) Schematic representation of structure of internal and external water conveyance substrate. (c) Schematic comparison of structure of a loofah sponge biochar evaporator. Reproduced with permission from ref. 42. Copyright (2022) Elsevier Inc.

loofah sponge biochar surface, light makes a constant reflection between the tight pore structure, thereby increasing the vibration frequency of the carbon lattice and increasing loofah sponge biochar's photothermal conversion efficiency. In addition to this, higher porosity facilitates channels for efficient water and steam flow and enhances water evaporation. The FTIR spectrum of towel gourd complex biochar is shown in Fig. 12d, which contains prominent peaks located at 1100, 1600, and 3430 cm^{-1} corresponding to C–O, C═O, and N–O/N–H. By performing carbonization in loofah sponge, hydrophilic groups (N–O and N–H), which contain higher nitrogen content, are lost. However, some of the oxygen-containing functional groups still remain, namely C–O and C═O. Hydrophilic nature is favourable for water and steam transportation of towel gourd complex biochar. Fig. 12e represents the XPS survey spectra of natural loofah sponge and natural loofah sponge biochar, where the peaks corresponding to C 1s, N 1s, and O 1s are positioned at 285, 400, and 523 eV, respectively. The N 1s peak with lower intensity represents a lower content of nitrogen in the material. After performing carbonization, the carbon content in loofah

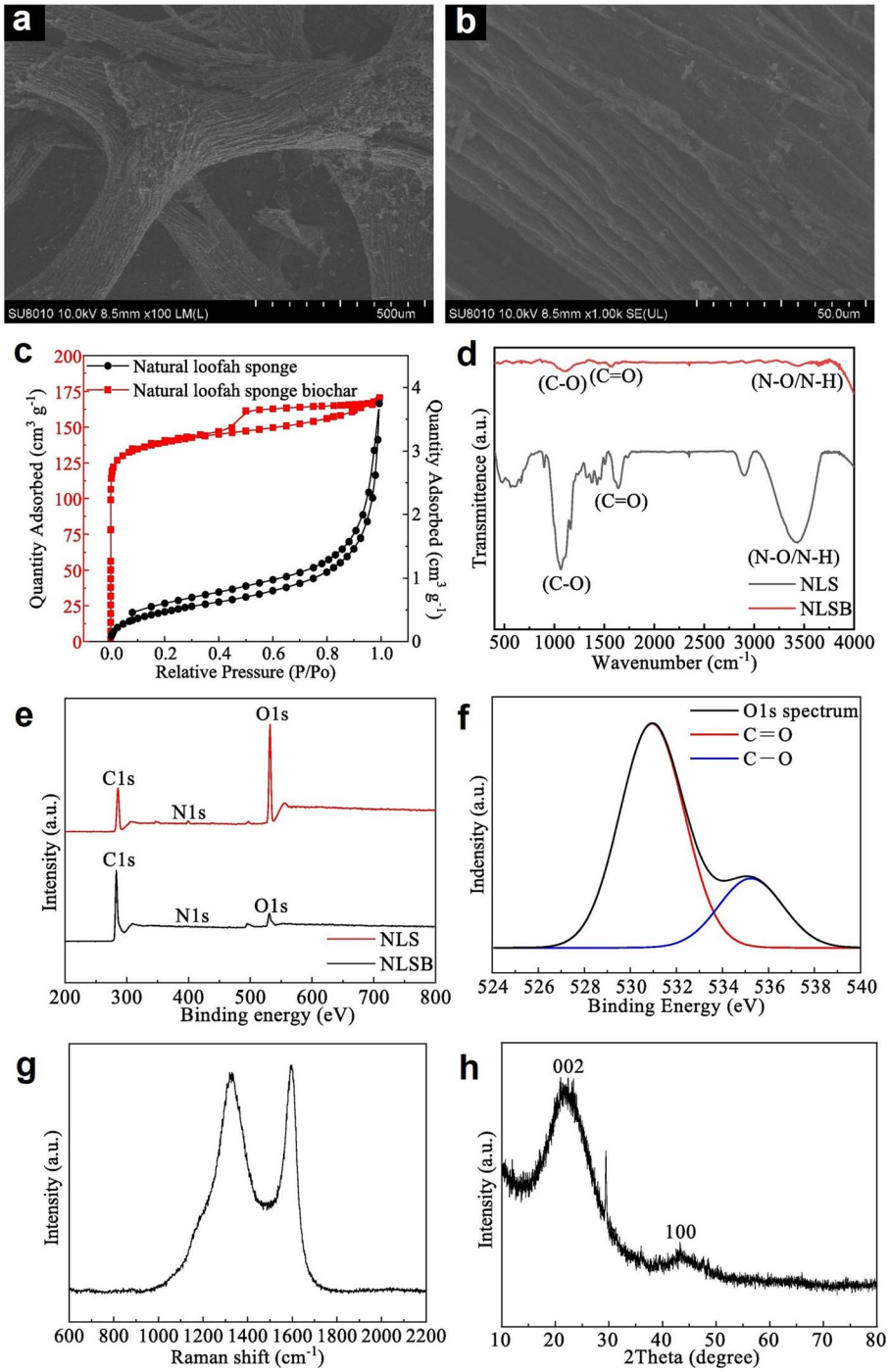

Fig. 12 (a) SEM image of loofah sponge biochar with ×100 magnification; (b) SEM image showing the surface structure in loofah sponge biochar with ×1000 magnification; (c) N_2 adsorption–desorption isotherms (d) FTIR spectra and (e) XPS survey spectra of natural loofah sponge and biochar of natural loofah sponge; (f) XPS deconvolution spectra fitting of O 1s; (g) Raman spectrum and (h) XRD pattern of loofah sponge biochar. Reproduced with permission from ref. 42. Copyright (2022) Elsevier Inc.

sponge is increased from 48.35% to 91.12% with an oxygen content of 6.79%. The O 1s deconvoluted XPS spectrum (Fig. 12f) indicates that the various oxygen-containing functional groups are C–O and C=O. Hydrophilic groups ensure an effective hydrophilicity in loofah sponge biochar, which transport steam and water effectively. The Raman spectrum of natural loofah sponge biochar is given in Fig. 12g. There are two prominent peaks located at 1330.4 and 1597.5 cm^{-1}, named as D-band and G-band, respectively. Here, the D-band, corresponding to atomic lattice defects, may be due to the presence of amorphous carbon or defective carbon in the structure. The G-band corresponds to in-plane stretching vibration in C atom of sp^2 hybrid, that represents crystalline carbon or ordered carbon. Graphitization degree in a carbon material is indicated

by the intensity ratio of D-band to G-band ($I_D : I_G$). A large I_D/I_G ratio represents a lower graphitization degree and the structure tends to be disordered. The XRD pattern of natural loofah sponge biochar is shown in Fig. 12h. In this pattern, there are broad diffraction peaks located at 21.9° and 43.3°, which correspond to 002 and 100 planes of graphite. A broadness in the peaks and reduced intensity reflect a reduced crystallinity and disordered structure in natural loofah sponge biochar. The as-prepared natural loofah sponge biochar possesses an interwoven structure with hollow fibers, and has a spacing of 10–100 μm. This higher pore diameter has negative impact on solar absorption, transfer of heat, and water transportation through the channels. From an analysis of the cross-sectional view, the authors observed that there exists a dense distribution of hollow spheres through the tubular holes having pore diameter varying between 4 and 10 μm. The tubular structure can be classified into transverse and longitudinal and the holes through the tubular structure make an arrangement in the transverse direction. The transport of water in the solar absorption layer is hindered with multiple pipe walls, and there is a reduction in the water transport layer. If the holes through the tubes are arranged longitudinally, the transmission rate of water is consistent along the hole direction, and thereby an increase in transmission rate can be achieved. Despite this, with respect to the slow rate of water transmission in tubular holes which are transversely arranged, the air in these holes introduces thermal resistance. This thermal resistance will hinder the transfer of heat from solar absorption layer to water. Most hollow fibers present in the solar absorption layer of natural loofah sponge biochar are arranged horizontally, greatly affecting the water transport and thermal conductivity of this absorption layer and hindering water evaporation. The authors of this work performed a desalination experiment with environmental conditions such as temperature of ~26 °C and humidity of ~35%. Here, the sunlight is obtained using a solar simulator and indoor evaporation experiment is performed with light intensity of 1000 W m^{-2}. From this experiment, it is observed that the natural loofah sponge biochar interfacial evaporator rate is 2.85 times that of normal seawater, reaching a maximum evaporation rate of 1.284 kg m^{-2} h^{-1}. This rate is found to be lower than that of a squashed natural loofah sponge biochar interfacial evaporator, which was about 1.565 kg m^{-2} h^{-1}. The evaporation rate of this squashed natural loofah sponge biochar interfacial evaporator is 3.64 times that of normal seawater, indicating the effective utilization of towel gourd biochar in the interface evaporation. Solar reflection and transmission losses for the natural loofah sponge biochar and squashed natural loofah sponge biochar were found to be 14.77% and 10.79%, respectively. The actual evaporation efficiency of the natural loofah sponge biochar was 61.37% whereas it was 80.66% for the squashed natural loofah sponge biochar. The evaporation efficiency of natural loofah sponge biochar is 61.37%, which is lower than the theoretical evaporation rate predicted (70.74%). This is due to the occurrence of a network architecture in the natural loofah sponge biochar and a reduced longitudinal water conveyance capacity. This leads to more dissipation of heat in the boundary between solar absorption layer and water conveyance architecture, which is not utilized in the evaporation of water. This study showed that by using natural loofah sponge biochar, high efficiency can be achieved while using it in solar interfacial evaporator with a reduced cost and showing scalability.

The first and foremost importance is given the ways to improve the solar desalination efficiency of these loofah sponges by increasing the solar absorption. This has resulted in the use of carbonaceous materials to combine with natural loofah sponge. With respect to the higher light absorption efficiency of graphene oxide and reduced graphene oxide, loofah sponge can be incorporated with these materials by preparing composite structures. The preparation of loofah sponge with reduced graphene oxide using a facile hydrothermal approach has been reported recently.[62] In a typical experimental procedure, the loofah sponge was cut into pieces and washed with ethanol and DI water. In order to prepare a loofah sponge/graphene oxide composite, the cleaned loofah sponge pieces were immersed in graphene oxide suspension and kept at a temperature of 20 °C for 12 h to create an ice-containing bulk component. Later, this bulk component was freeze-dried to remove water and a loofah sponge@graphene oxide aerogel was prepared. Further, this aerogel was transferred into a Teflon-lined vessel and kept at a temperature of 150 °C for 10 h to execute hydrothermal reaction of loofah sponge in order to reduce the graphene oxide. In this study, the authors of this work produced a partially modified loofah sponge with hydrophobic reduced graphene oxide in which there is a Janus architecture containing hydrophilic–hydrophobic components. This partially modified loofah sponge with reduced graphene oxide possesses a two-layer Janus structure, having a bottom layer of unmodified loofah sponge containing macropores with a mean diameter of 500 μm, whereas the upper layer of reduced graphene oxide-modified loofah sponge exhibits a multi-scale porous architecture. Here, the unmodified bottom layer has a macroporous architecture created through interweaving fibers with diameter ranging between 100 and 200 μm. On the other hand, the upper layer has a hierarchical structure inferred from modification of reduced graphene oxide on hydrothermally synthesized loofah sponge fibers, while maintaining the structural qualities. The pore diameter of the upper-layer portion is calculated to be 100 μm, which is less than that of the lower layer. Hierarchical structure of the upper layer favours solar absorption by large amounts of refraction and reflection. The loofah sponge/graphene oxide composite was further used for a solar-driven interfacial water evaporation experiment using seawater. The change in mass of seawater with respect to time was calculated and an evaporation rate of 0.24 kg m^{-2} h^{-1} was obtained at 1 sun illumination. The partially modified, hydrothermally synthesized loofah sponge with graphene oxide exhibits a higher evaporation rate of 1.54 kg m^{-2} h^{-1}. But the loofah sponge, reduced graphene oxide and hydrothermally synthesized loofah sponge fibers exhibited evaporation rates of 0.82, 1.02, and 1.07 kg m^{-2} h^{-1}, respectively. The efficient salt resistance introduced by the hydrophobic side of the hydrophilic-hydrophobic Janus architecture helped in achieving good desalination efficiency.[62]

Capacitive deionization using porous electrode material is an efficient electrochemical technology for the desalination of brackish water. Nanoporous carbon materials like carbon aerogel, graphene, carbon nanofiber and activated carbon are indispensable and prevalent for wide application due to their large surface area, prominent adsorption capacity, and good stability. High-quality activated carbon can be synthesized from natural loofah sponge.[63] In a typical procedure, the loofah sponge was washed three times with deionized water and dried at 105 °C overnight. Later, it was taken in a porcelain boat and transferred into a tubular furnace, maintaining the temperature at 600 °C for 1 h, and loofah sponge biochar was obtained. Further, this loofah sponge biochar was activated in KOH medium by mixing KOH and loofah sponge biochar at different ratios using deionized water and further annealed at a temperature of 800 °C for 1 h under nitrogen atmosphere. In order to remove the insoluble components, the resulting black powder was immersed in dilute HCl and washed several times with deionized water and dried in vacuum for 12 h at 80 °C. The biochar to alkali ratio was varied such as 1 : 1, 1 : 2, and 1 : 4 and the authors of this work prepared different combinations of resultant product. By using SEM analysis, it was observed that multi-channelled carbon product crushed to short fibers with irregularly branched short fibers holds a length of 6–75 μm and width of 2–40 μm. The channel possesses a thickness of 0.1 μm. Large numbers of micro-holes were present in the activated carbon with a ratio of 1 : 4 having diameters of 2–5 μm, which indicates that an increase in KOH-to-biochar ratio helped in improving the microstructure. These investigations indicated a net-like fibrous vascular system in loofah sponge and a high fiber fraction, like cellulose, lignin, and hemicellulose. This porous architecture having smooth and straight channels on a micrometer scale has prominent applications in boosting transfer of electrolyte ions in solution, being favourable for deionization. Electrosorptive desalination characteristics of the materials were evaluated using a potentiostat by performing membrane capacitive deionization at 1 V with 10 mM NaCl having initial conductivity of 1025 μS cm^{-1}. In the electrosorption stage, there are typical curves, characterizing rapid removal of salt ions from the aqueous solution. The removal efficiency of loofah sponge-derived biochar-based activated carbon is 19.8%, 19.5%, and 40.1% for 1 : 1, 1 : 2, and 1 : 4 samples, respectively, which indicates that the sample with a ratio 1 : 4 has higher electrosorption capacity. Here, a fluctuation in pH is not affected the membrane capacitive deionization process. In addition to this, an activated carbon electrode is a necessary component in membrane capacitive deionization, which is attained through the application of bias voltage. For desorption, there is an increase in conductivity and the recovery rates are 90%, 84%, and 97% for 1 : 1, 1 : 2, and 1 : 4 samples, respectively. These results show an efficient electrosorption behaviour for regeneration at a ratio of 1 : 4. With an increase in ion concentration to 10 mM, this particular ratio (1 : 4) leads to a high electrosorption capacity of 22.5 mg g^{-1} for brackish water. The presence of uniquely oriented micrometer-scale channels provides an efficient utilization of the available electrode surface area. These obtained results demonstrate the feasibility of resource recovery from loofah sponge fiber, being a promising candidate for water desalination, and such environmentally friendly solutions are highly recommended. To avoid the problems associated with the electrode material's reduced salt adsorption capacity and lower charge efficiency for operation, it is required to prevent co-ion expulsion during charging. In addition to this, a reverse potential is applied for electrode regeneration. A demerit of this method is the re-adsorption of ions to the opposite electrode during the capacitive deionization process.[63]

To improve the features of membrane capacitive deionization, electrode materials are developed with large surface area, uniform pore-size distribution, and good electrical conductivity. An in-depth study was conducted to evaluate the influence of applied potential and concentration of salt-on-salt adsorption capacity, energy consumption, and charge efficiency in a membrane capacitive deionization system with loofah sponge-derived biowaste carbon.[64] Here, a commercially available loofah sponge was cut into pieces and kept for carbonization under argon atmosphere for 1 h at 800 °C. In order to activate the loofah sponge-derived carbon, it was later mixed with KOH in 1 : 2 ratio in 30 mL of deionized water for 10 h and dried at 80 °C in an oven. The prepared mixture was further heated to a temperature of 800 °C at a rate of 5 °C min^{-1} for 1 h. A schematic diagram of the membrane capacitive deionization cell utilizing a loofah sponge-derived activated carbon electrode is shown in Fig. 13. A typical membrane capacitive deionization system is composed of an ion exchange membrane pair kept in front of the loofah sponge-derived activated carbon electrodes with a nylon spacer. Here, the authors of this work prepared electrode materials with a thickness of 200 μm and an overall electrode mass (carbon black, active material, and polyvinylidene difluoride) of 100 mg. The authors evaluated the electrosorption characteristics before and after performing KOH chemical activation. After carbonization and KOH activation, there exists a porous architecture in the loofah sponge-derived activated carbon whereas pristine loofah sponge was composed of interconnected fiber networks. The presence of the interconnected porous architecture introduced an effective pathway for rapid diffusion of ion species. With respect to the higher surface area and hierarchical pores with uniform pore-size distribution, the loofah sponge-derived activated carbon exhibited a large number of active sites for ion adsorption.

To evaluate the desalination characteristics, a positive potential was introduced to the membrane capacitive deionization system across two electrodes in the charging process for ion adsorption from solution consisting of a known NaCl concentration and a negative potential for the electrode discharge for the ions expelled in the waste stream. The desalination performance of loofah sponge-derived activated carbon at 2500 mg L^{-1} initial concentration within a potential window of 0.8–1.2 V in NaCl solution is shown in Fig. 14a. With the applied potential, there exists a sharp reduction in solution conductivity initially for charging and then adsorption attains equilibrium with a reduction in conductivity until reaching a plateau. Fig. 14b presents a positive correlation of transient current response with respect to an increase in potential. Fig. 14c shows the salt adsorption capacity of loofah sponge-

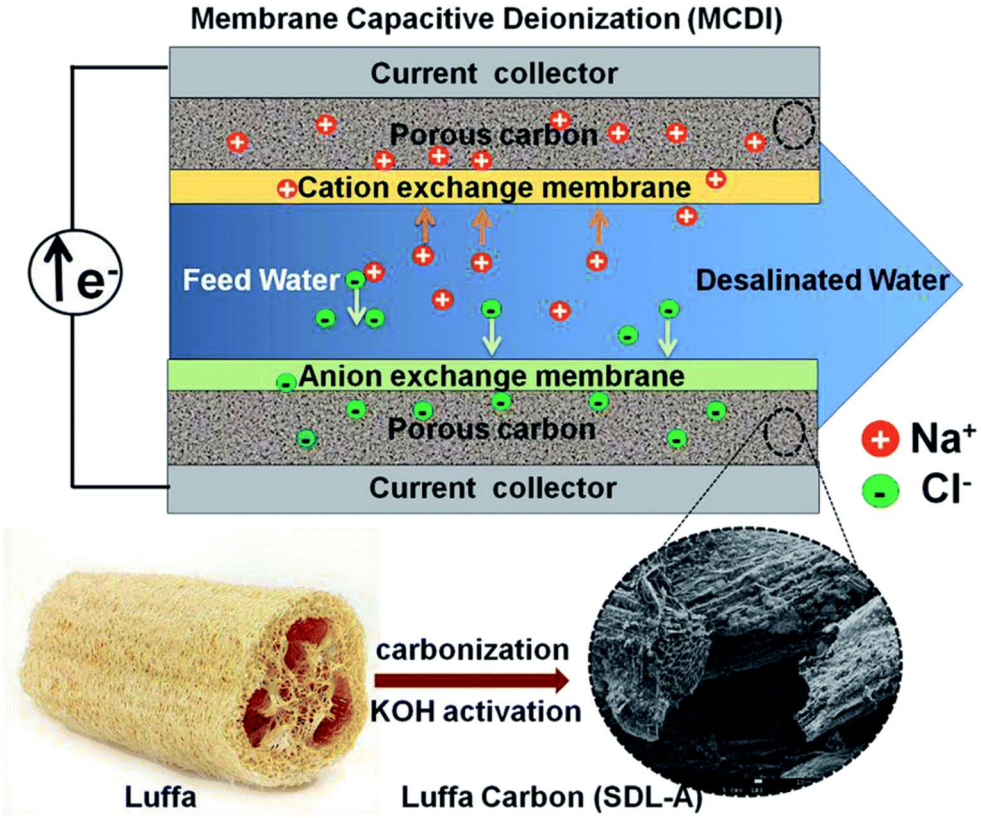

Fig. 13 Schematic representation of the synthesis process of loofah sponge-derived carbon after activation (represented in the figure as SDL-A) for membrane capacitive deionization. Reproduced with permission from ref. 64. Copyright (2019) Royal Society of Chemistry.

derived activated carbon electrode at various applied potentials. By varying the applied potential from 0.8 to 1.2 V, the salt adsorption capacity increased from 23 to 38 mg g^{-1}, which indicates that higher cell potential enhances the electrosorption capacity. The phenomena observed are due to the occurrence of stronger electrostatic force and formation of thicker electrical double layer with an increase in voltage. The cyclic stability of loofah sponge-derived activated carbon electrode at 2500 mg per mL NaCl solution for charge/discharge cycles is found to be good and a major reduction in removal capacity was observed (Fig. 14d). This result confirms that the activated carbon electrode can be completely regenerated and it is possible to reuse without any significant degradation. Hence, it is a potential electrode material for membrane capacitive deionization.

An increase in the charge efficiency from 83 to 87% with respect to the increase in applied voltage from 0.8 to 1.2 V in NaCl solution for loofah sponge-derived activated carbon and from 70 to 80% for the carbon without activation are obtained. At an applied potential of 1.2 V, the salt adsorption capacity for the loofah sponge-derived activated carbon is 38 mg g^{-1} at 80% charge efficiency. The presence of both mesopores and micropores in the activated carbon electrode helps in reducing the NaCl resistance by the diffusion of it through pores and the ion adsorption is enhanced by the large surface area. These results indicate the feasibility of the KOH-activated electrode as an efficient material for membrane desalination.

A composite of two-dimensional layered MoS_2 and highly porous loofah sponge and a glucose-derived carbon was prepared and used as water evaporator.[65] The lightweight and cost-effective loofah sponge holds a highly macroporous architecture and it possesses an open network. The authors of the present work prepared loofah sponge containing MoS_2 and amorphous carbon particles through a hydrothermal approach, by combining sodium molybdate dihydrate, thiourea and glucose for a period of 6 h at a temperature of 180 °C. To this solution, a cleaned loofah sponge is introduced. After completing the experiment, the resultant product is washed and kept for further analysis. In addition to this, the authors prepared MoS_2/carbon hybrid by a hydrothermal approach without using glucose. The ripe form of loofah sponge is tough and it consists of hoop walls with central spines, as shown in Fig. 15a. After removing the central spines, the remaining portion of the circular wall is unfolded to a porous and flexible plate. The internal and external portions of sidewall present in loofah sponge possess various porosity and orientation of fibers. The inset image of Fig. 15a shows a thicker and sparser internal wall, but the external wall is observed to be denser having intertwined and slender fibers. It was observed that the loofah sponge taken for analysis consists of a large number of open micropores present between numerous fibers (Fig. 15b), but loofah fiber exhibits a wrinkled and rough surface. The SEM cross-sectional image of loofah sponge shows well-aligned

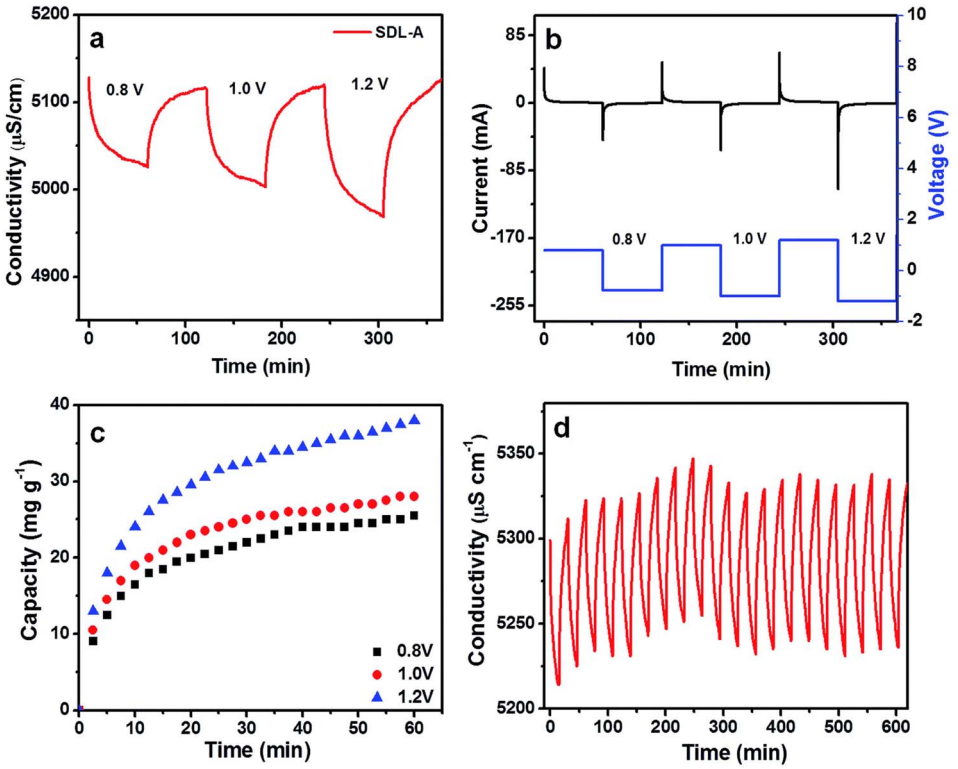

Fig. 14 (a) Electrosorption character of loofah sponge-derived activated carbon with respect to different voltages in NaCl solution with initial concentration of ~2500 mg L^{-1} having flow rate of 50 mL min^{-1} and (b) the corresponding current and voltage response. (c) Removal capacity of salt for a loofah sponge-derived activated carbon electrode at a voltage range 0.8–1.2 V in NaCl solution having an initial concentration of ~2500 mg L^{-1}. (d) Curve of deionization and regeneration for loofah sponge-derived activated carbon in 2500 mg per L NaCl solution for an applied voltage of 1.2 V. Reproduced with permission from ref. 64. Copyright (2019) Royal Society of Chemistry.

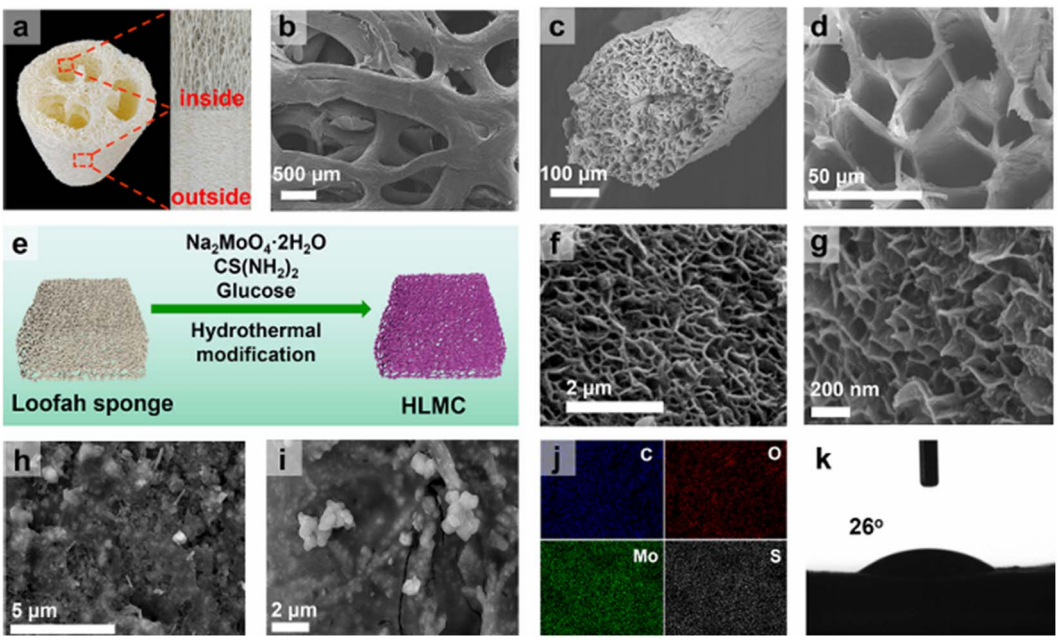

Fig. 15 (a) Images of loofah sponge fibers showing different microstructure outside and inside. SEM images of loofah fiber showing (b) macroporous fiber, (c) microporous fiber, (d) microchannels in loofah fiber. (e) Schematic representation of hydrothermal procedure to synthesize HLM. (f and g) SEM images of HLM surface at two magnifications. (h and i) SEM images of HLMC surface at two magnifications. (j) EDS elemental mapping images of HLMC for the elements Mo, S, O, and C. (k) Water contact angle measurement of HLMC. Reproduced with permission from ref. 65. Copyright (2023) American Chemical Society.

abundant porous microchannels having diameters of 10–30 μm (Fig. 15c and d). These porous microchannels and the open macropores in the fibers not only facilitate spontaneous transportation of water upwards with the help of capillary force, but also provide circulation of water and salt inside the cylindrical evaporator. To realize loofah sponge having higher absorption rate for sunlight with a high conversion capacity of solar-thermal energy, it is decorated with MoS_2 sheets and carbon particles by immersing it in a precursor solution and followed by hydrothermal synthesis at a temperature of 180 °C (Fig. 15e). The as-obtained composite is labelled as HLMC. The loofah sponge is darker after undergoing the hydrothermal reaction and MoS_2 sheets are decorated *in situ* on the hydrothermally treated loofah fiber surface (Fig. 15f). The MoS_2 sheets are observed to be small and aligned tightly as a surface coating (Fig. 15g), which leads to a rough surface in comparison with natural loofah fiber. In addition to this, amorphous carbon particles are introduced *via* dehydrogenation and dehydration of glucose during the hydrothermal reaction, which results in the formation of a nodule-architectured loofah composite (Fig. 15h). Here, some amorphous carbon particles having a size of ~0.7 μm were clumped to form carbon clusters (Fig. 15i). The EDS elemental mapping images present a uniform distribution of individual elements in the composite (Fig. 15j). Fig. 15k presents the water contact angle measurements of the composite from which a contact angle of 26° is observed, validating the hydrophilic nature of the composite.

The authors of this work investigated the relationship between the water evaporation capability of the HLMC evaporator and its exposed heights. After evaluating this, they optimized the water evaporation rate as 3.45 kg m^{-2} h^{-1} under a solar irradiation power of 1 sun. From this optimized combination, water purification and the salt-resistance

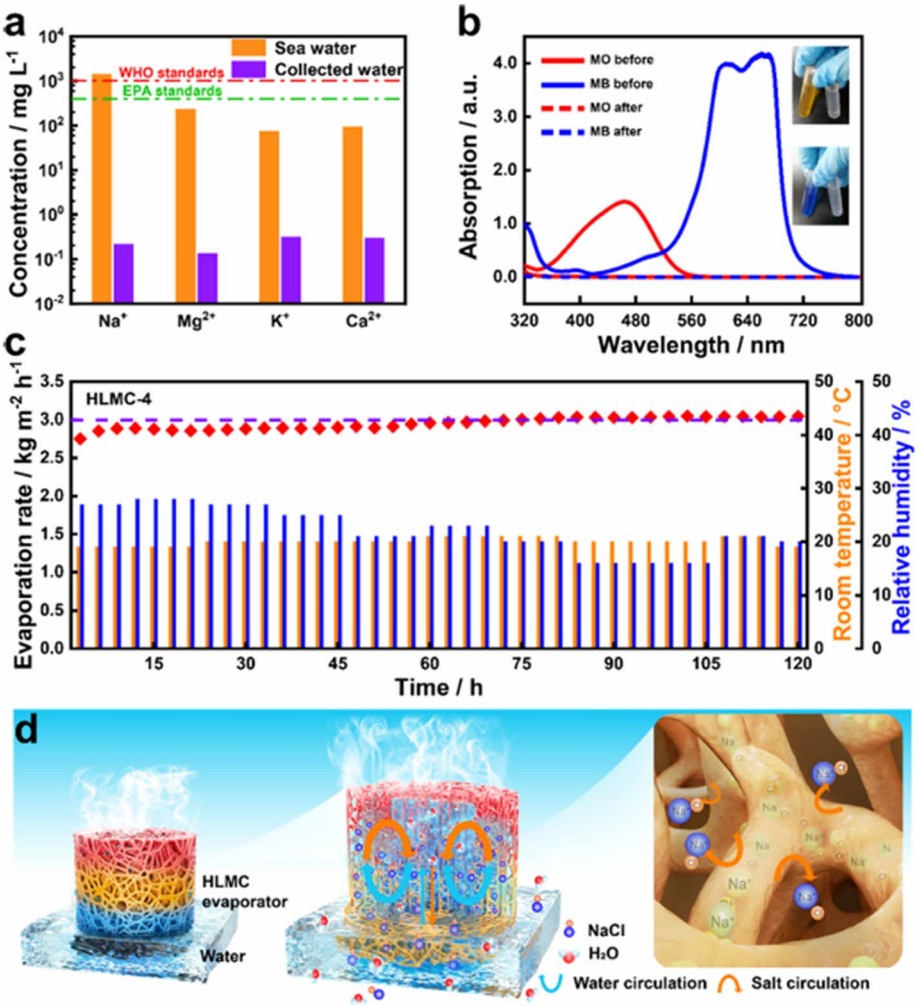

Fig. 16 (a) Ionic concentration of different ions in actual seawater and desalinated water. The colored lines represent WHO and EPA standards for drinking water. (b) Ultraviolet-visible absorption spectra of methylene blue and methyl orange with HLMC before and after evaporation under irradiation of 1 sun (insets are digital image before and after irradiation). (c) Long-term evaporation test for the HLMC evaporator using 3.5 wt% NaCl under continuous irradiation for 120 h with related humidity and room temperature information. (d) Schematic representation of generation of solar steam and the desalination mechanism for HLMC. Reproduced with permission from ref. 65. Copyright (2023) American Chemical Society.

capability of the solar-driven evaporator were evaluated. The concentration of ions such as Na^+, Mg^{2+}, K^+, and Ca^{2+} present in the water evaporated by the HLMC evaporator is found to be much smaller than seawater content (Fig. 16a), which is in complete compliance with the drinking water standard of WHO and Environmental Protection Agency (EPA). The resistances of seawater before and after performing solar steam generation are found to be 143.9 kΩ and 1.72 MΩ, respectively. The resistance is increased due to reduced ion concentration in the seawater after evaporation using the solar-driven HLMC evaporator. In addition to this, HLMC is capable of removing organic dyes from aqueous solution *via* the solar steam generation route. The aqueous solution absorption for dyes before and after the solar-driven purification is analyzed with ultraviolet-visible absorption spectroscopy and the obtained spectra are shown in Fig. 16b. It can be observed that the spectra show elimination of strong absorption peaks introduced by methylene blue and methyl orange, representing clean water generation. The long-term stability results of the HLMC evaporator to desalinate seawater continuously for 120 h is given in Fig. 16c. The efficient solar steam performance and excellent salt-resistant capability of the HLMC evaporator resulted from the natural macroporous architecture of loofah sponge. The hydrophilic nature of loofah sponge coupled with the microporous structure facilitates rapid absorption of water and its upward transport. During the desalination process, the continuous evaporation of water left behind the salt on the composite and crystallization of salt occurred upon localized surface heating. A schematic diagram representing the water desalination using HMLC with the mechanism is depicted in Fig. 16d in which the uneven structure of the evaporator tends to produce a gradient water distribution transfer in the evaporator. The salt accumulation at the side surface of the HLMC evaporator is due to the poor water solubility and the concentration of salt in the upper layer is higher than in its bulk water through rapid evaporation of water on the evaporation surface. A difference in the salt concentration (higher and lower) leads to convection and diffusion of salt. In addition to this, the concentration of salt gradient accelerates the exchange of mass between macropore and micropore channels to prevent possible salt accumulation over the evaporator surface.

MXenes is a collective name given to transition metal carbides, metal nitrides, and carbonitrides. They are two-dimensional layered materials that find applications in various fields such as energy,[66,67] catalysis,[68] water purification,[69] *etc.* MXenes possess large surface area, good electronic conductivity, tunable photothermal properties, *etc.* The photothermal property of loofah sponge-based biomass materials can be modified by incorporating MXenes within them. A surface treatment of coating with MXene is found to be an efficient approach to increase solar absorption. In the family of MXenes, Ti_3C_2 MXene has an internal light-to-heat conversion efficiency of ~100%, indicating its potential for use as a photothermal material in solar steam production. Due to the semi-metallic nature of Ti_3C_2 MXene, the photothermal conversion process is a localized surface plasmon resonance phenomenon. But the smooth surface of MXene and spontaneous restacking hinder water transport and the escape of water vapor. Hence, a modification is required on the surface of MXene. The utilization of loofah sponge as a 3D microporous structure as solar evaporator with a Ti_3C_2–MnO_2 surface coating was reported previously.[70] In a typical experimental procedure, MXene was synthesized by a hydrofluoric acid etching method and further mixed with MnO_2 powder using isopropyl alcohol. Six samples were prepared by varying the Ti_3C_2 to MnO_2 mass ratio and the mean absorption was evaluated. A sample prepared using $Ti_3C_2 : MnO_2 = 2:5$ (in mg mL^{-1}) is found to be optimal to achieve the best performance. In a typical procedure, MXene and MnO_2 were dissolved in isopropyl alcohol separately and ultrasonicated for 4 h. Later, MXene (60 mL) and MnO_2 (40 mL) were mixed in a beaker and magnetically stirred at 600 rpm for 2 h. Further, the precleaned loofah sponge was dip-coated several times in the as-prepared dispersion to obtain a uniform coating. Later, the sample was kept at 65 °C in an oven for 6 h. A schematic diagram representing the synthesis method of the Ti_3C_2–MnO_2-loofah sponge hybrid is given in Fig. 17a. Finally, a steam evaporation experiment was conducted using the as-prepared Ti_3C_2–MnO_2-loofah sponge hybrid

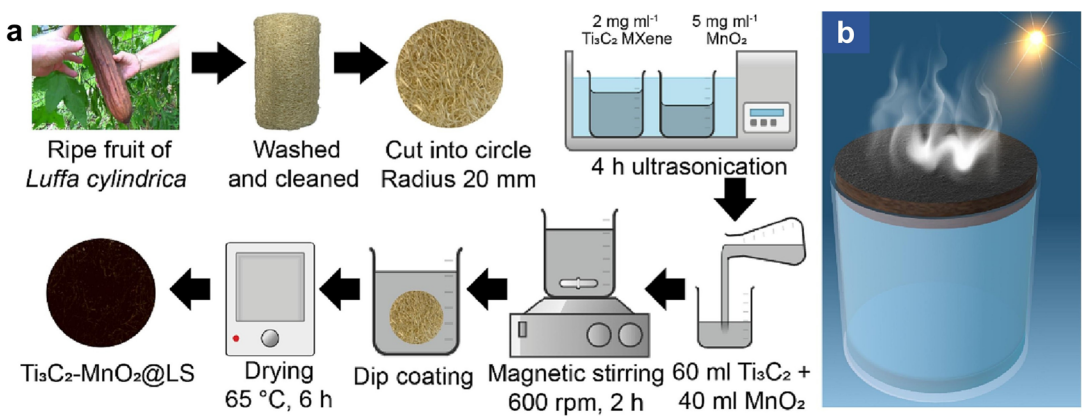

Fig. 17 (a) Schematic representation of the synthesis process of Ti_3C_2–MnO_2-loofah sponge hybrid. (b) Illustration showing the generation of solar steam using the Ti_3C_2–MnO_2-loofah sponge hybrid. Reproduced with permission from ref. 70. Copyright (2023) Elsevier Inc.

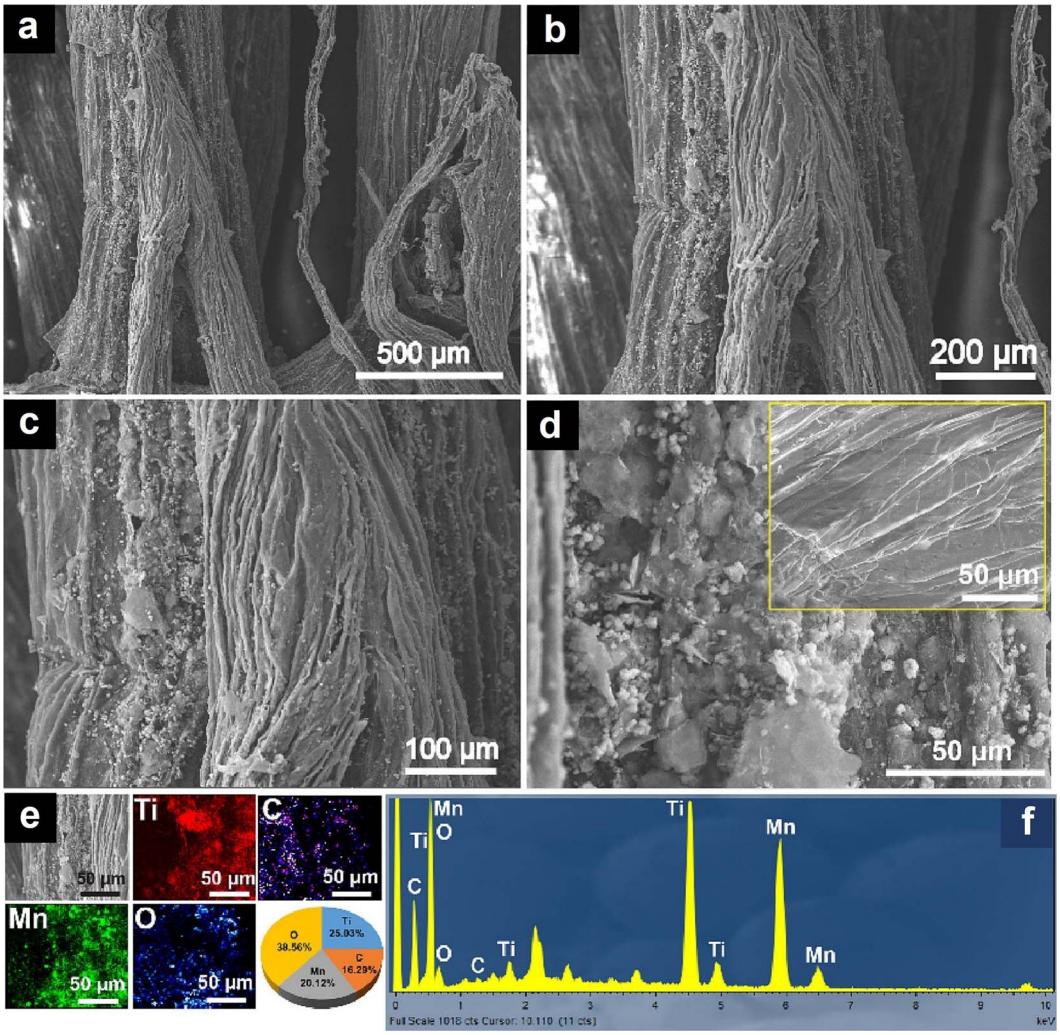

Fig. 18 (a–d) SEM images of Ti_3C_2–MnO_2-coated loofah sponge with various magnifications. Inset of (d) shows pristine loofah sponge. (e) EDS elemental mapping. (f) EDS spectrum showing elemental analysis. Reproduced with permission from ref. 70. Copyright (2023) Elsevier Inc.

by placing it on water in a beaker (Fig. 17b) and exposed to sunlight.

When compared with the pristine natural loofah sponge, this hybrid material exhibits efficient light absorption characteristics. The surface morphology of this hybrid material was examined using SEM imaging and the SEM images at different magnifications are shown in Fig. 18a–d. Natural loofah sponge possesses a fiber-like porous architecture, feasible for water transport from underneath bulk water. With the coating of Ti_3C_2–MnO_2 over the natural loofah sponge, its surface is completely covered with Ti_3C_2–MnO_2 nanoparticles. In comparison with the smooth surface of natural loofah sponge (inset of Fig. 18d), the surface of hybrid material is found to be rough, which is beneficial for reducing the light reflection. The porous architecture of natural loofah sponge helped in attaining good surface coverage of the Ti_3C_2–MnO_2 nanoparticles during dip coating. From the SEM-EDS elemental mapping images (Fig. 18e), it can be observed that there is a continuous and homogeneous distribution of Ti, Mn, C, and O elements. The composition of various elements present in the loofah sponge-Ti_3C_2–MnO_2 hybrid material is available from the SEM-EDS spectrum given in Fig. 18f and found to be 25.03%, 20.12%, 16.29%, and 38.56% for Ti, Mn, C, and O, respectively.

Heat confinement was evaluated by measuring the cross-sectional distribution of temperature of the beaker with and without the Ti_3C_2–MnO_2 coating on natural loofah sponge floating on the air–water interface by using an infrared camera under irradiation of 1 sun. As given in Fig. 19a, upon 30 min illumination, a beaker containing water showed a homogeneous distribution of temperature throughout the volume (55.1 °C). Under the same conditions, in the case of the beaker with water and loofah sponge-Ti_3C_2–MnO_2 hybrid material floating on it, a different thermal profile was exhibited over the volume. The infrared camera images showed that the portion containing the loofah sponge-Ti_3C_2–MnO_2 hybrid material dipped inside the water exhibited a higher temperature (63.9 °C) when compared to that of the portion of water at the bottom (27.3 °C). Further, the desalination performance of the loofah sponge-Ti_3C_2–MnO_2 hybrid material was evaluated with collected seawater and NaCl having higher concentrations

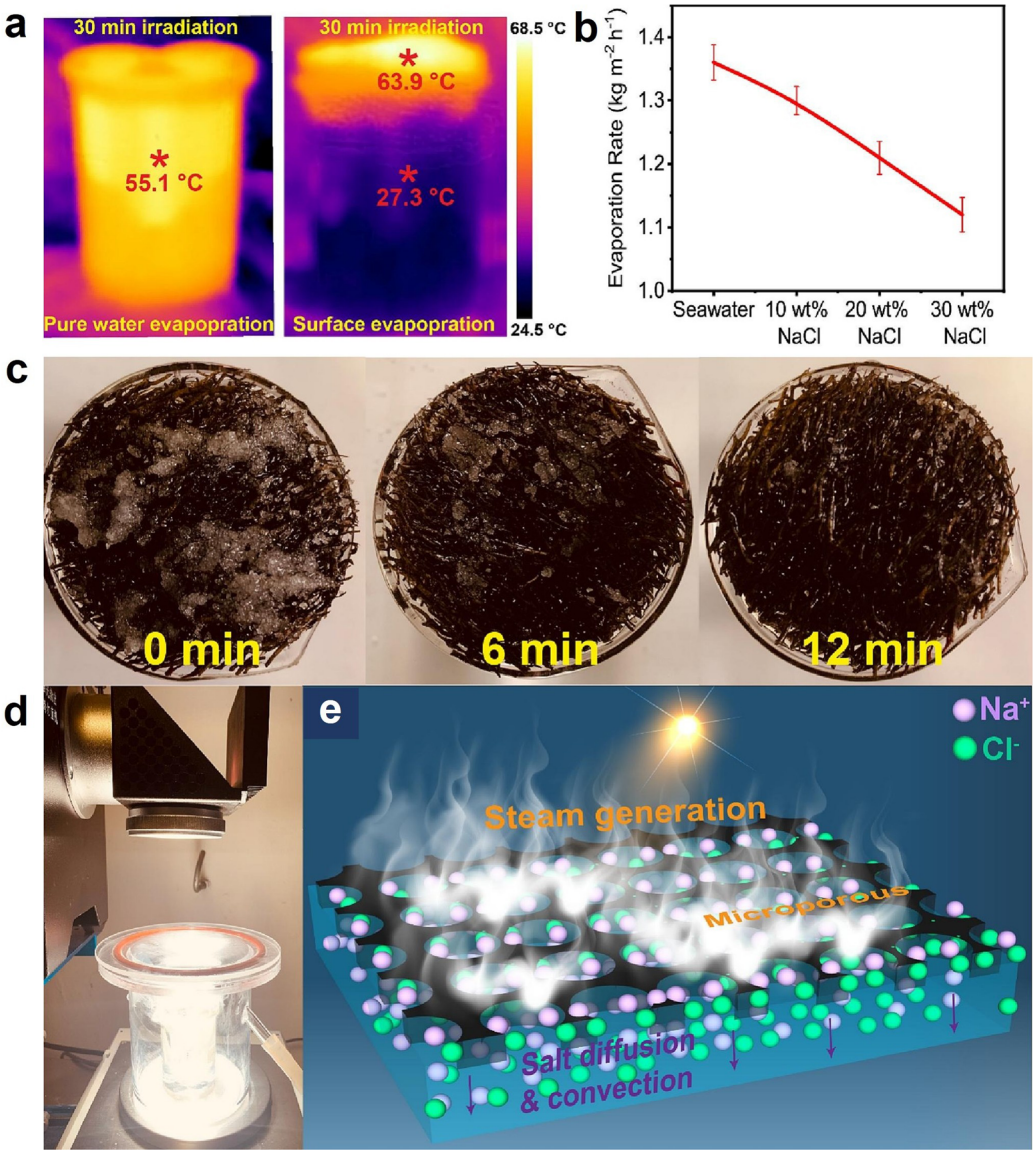

Fig. 19 (a) Infrared camera images of side view of temperature distribution of a system having only water and Ti_3C_2–MnO_2@loofah sponge hybrid after 30 minutes of irradiation. (b) Rate of solar evaporation by Ti_3C_2–MnO_2@loofah sponge hybrid with respect to variation in salinity value (seawater, 10, 20, 30 wt%). (c) Salt resistance progression under irradiation of 1 sun. (d) Picture of homemade setup used for desalination of seawater. (e) Schematic representation of possible salt rejection mechanism of Ti_3C_2–MnO_2@loofah sponge hybrid. Reproduced with permission from ref. 70. Copyright (2023) Elsevier Inc.

(prepared using 10, 20, and 30 wt% NaCl in water) and the solar evaporator was illuminated with 1 sun. From Fig. 19b, it is clear that the rate of evaporation reduces with increasing NaCl concentration. This is due to the water vapour pressure reducing with an increase in salinity. Seawater evaporation rate was higher than 1.3 kg m^{-2} h^{-1} whereas it was ~1.1 kg m^{-2} h^{-1} for 30 wt% of NaCl solution, indicating the efficient desalination performance of the loofah sponge-Ti_3C_2–MnO_2 hybrid material. As shown in Fig. 19c, when there was a 5 g NaCl crystal placed directly on top of the loofah sponge-Ti_3C_2–MnO_2 hybrid material and irradiated with a solar illumination of 1 sun, the NaCl was found to be gradually dissolved in 12 minutes. This confirms a prominent salt ion diffusion backflow feature of the loofah sponge-Ti_3C_2–MnO_2 hybrid material. The salt rejection property of a membrane in solar desalination is a prerequisite since the accumulation of salt will block the transportation channels of water and hinder solar absorption, resulting in a reduced evaporation efficiency. This salt ion diffusion backflow can be described as follows. Firstly, loofah sponge has a porous architecture with linked channels for fast water transport and escape of vapour. The hydrophilic feature of loofah sponge makes it moist, allowing adequate flow of water by capillary action and faster steam generation. There is a difference in concentration of salt between higher salt region and bulk water which introduces convection and diffusion, thereby producing a reduction in the concentration of salt in

the solar evaporator and preventing salt deposition. To illustrate the practical application of seawater and purification of wastewater, solar desalination was conducted in a homemade set-up having natural seawater and simulated wastewater, as shown in Fig. 19d. This vapor will condense in the chamber and it is possible to collect it for further use. Fig. 19e indicates that with respect to the naturally occurring microporous structure in loofah sponge, it exhibits an efficient salt ion diffusion backflow phenomenon. It can be said that the loofah sponge-Ti_3C_2–MnO_2 hybrid material can efficiently prevent salt deposition during desalination and hence it is a potential membrane for solar evaporators. A novel biodegradable loofah sponge-based nanocomposite comprising MXene and RuO_2 has been reported recently. The loofah sponge/MXene@RuO_2 nanocomposite was synthesized by a hydrothermal method.[71] The as-prepared nanocomposite exhibits a rough architecture having reduced light reflection. In addition to this, the loofah sponge/MXene@RuO_2 nanocomposite exhibits an enhanced absorption of light and helps in attaining a high evaporation rate for interfacial solar desalination. The loofah sponge/MXene@RuO_2 nanocomposite exhibited an evaporation capacity of 1.5 kg m^{-2} h^{-1} under an illumination of 1 sun. The total energy absorbed by this composite is about 90.85% and the overall heat loss is only 9.15%. Moreover, the authors of this work tested the desalinated water and observed that there is a noticeable reduction in the concentration of ions and salinity. Hence the loofah sponge/MXene@RuO_2 nanocomposite demonstrated its potential for solar interfacial desalination.

A $Ti_3C_2T_x$/graphitic carbon nitride/activated carbon@loofah sponge nanocomposite was synthesized by a hydrothermal approach at a reaction temperature of 140 °C for 16 h and used as a solar absorber for water desalination experiments.[22] In a typical procedure, graphitic carbon nitride is prepared by high-temperature pyrolysis and MXene is synthesized from its MAX

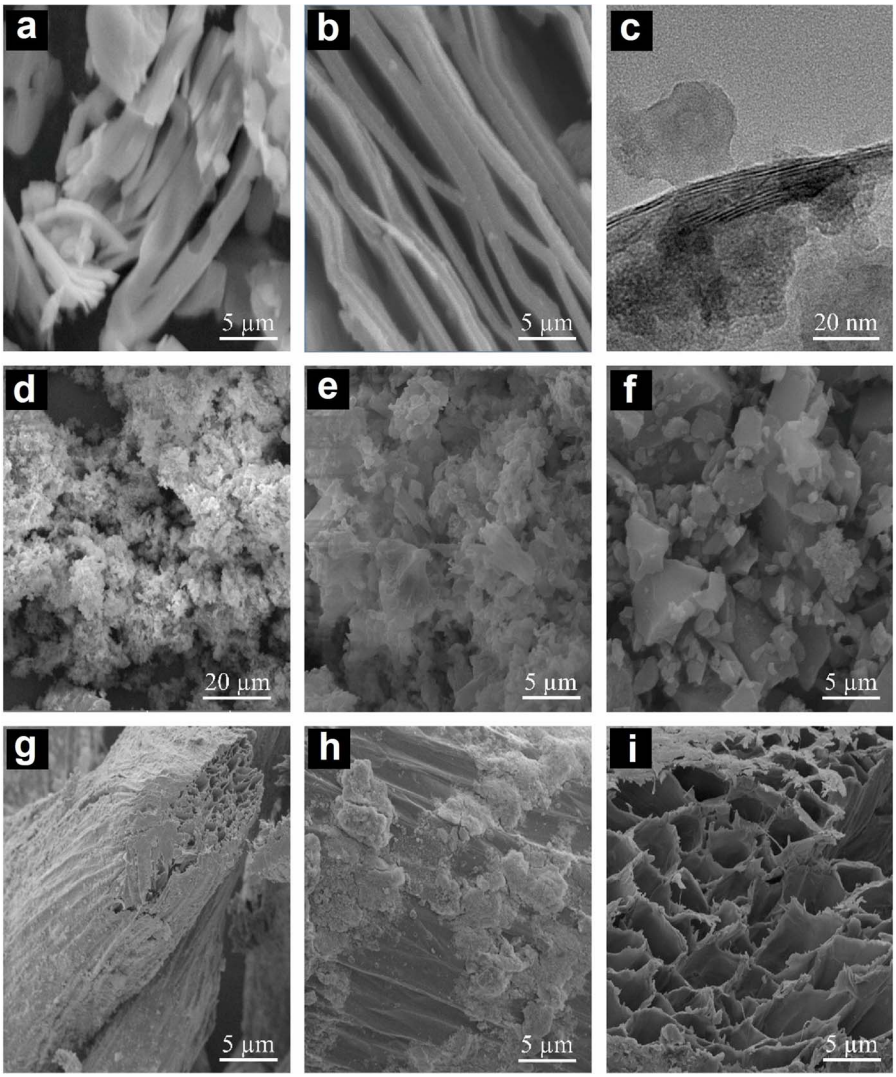

Fig. 20 (a) SEM image of MXene. (b) FESEM image of MXene. (c) HRTEM image of MXene. (d and e) SEM images corresponding to graphitic carbon nitride. SEM images of (f) activated carbon and loofah sponge (g) before and (h) after being coated with graphitic carbon nitride. (i) SEM image of loofah sponge. Reproduced with permission from ref. 22. Copyright (2024) Elsevier Inc.

phase precursor by using etchants which contain acid and fluoride salts. The SEM image of MXene (Fig. 20a) shows a layered architecture and the FESEM image (Fig. 20b) presents a multilayered architecture with interlayer gaps. The aluminium layers are etched away from the MAX phase in order to obtain the MXene with a layered architecture. A high-resolution TEM image of MXene is shown in Fig. 20c presenting the crystalline nature with lattice fringes. The morphological features of graphitic carbon nitride are evaluated with SEM imaging and Fig. 20d and e presents the SEM images at two different magnifications. The SEM image of activated carbon is given in Fig. 20f and a porous architecture can be seen in the case of loofah sponge (Fig. 20g). An SEM image of loofah sponge after coating with graphitic carbon nitride is shown in Fig. 20h. Fig. 20i presents a SEM image of loofah sponge.

Here, the evaporator fabricated with this hybrid loofah sponge composite having 1.25 cm dimension displays efficient performance, which exhibits an evaporation rate of 2.6 kg m^{-2} h^{-1} and a high solar thermal efficiency of 96% under illumination of 1 sun. Efficient wetting helps in rapid water transportation through the microchannels in loofah sponge and achieves a high water evaporation rate. Jia and team prepared an evaporator from waste biomass which consists of MXene and a loofah sponge and further used it as a solar absorber for solar steam desalination.[72] The MXene/loofah sponge exhibits good light absorption and efficiency. The natural hydrophilicity and the presence of microchannels not only allow pumping sufficient water to the top layer for heating, but also prevent salt from accumulation on the evaporator surface. The photothermal evaporator delivers an evaporation rate of 1.57 kg m^{-2} h^{-1} and a solar-thermal conversion efficiency of 95.5%. The efficient salt rejection property exhibited by the natural loofah sponge-based nanocomposite/hybrid materials opens up new avenues to achieve improved performance for solar water desalination applications. From the present review, it is evident that natural loofah sponge-based membranes and derived components are potential active materials in desalination applications. In addition to this, in comparison with other conventional approaches of wastewater treatment, natural loofah sponge-based solar water desalination is an efficient route for the production of freshwater in a cost-effective and eco-friendly approach.

4. Future perspectives

With respect to economic development and growth in population, the need for freshwater resources is increasing. Sustainable and renewable means of freshwater production are not a requirement but a necessity for retaining life on Earth. Desalination technology has attracted great interest in the recent past due to its versatility, cost-effectiveness, and scalability. Seawater desalination is a viable method as seawater is a naturally abundant resource. Biomass-based water purification has attracted great interest due to its environmentally friendly feature coupled with safety for human life. Among the various biomass-based materials, natural loofah sponge is a low-cost material available as a membrane for desalination applications. From the present review, we found that natural loofah sponge as well as its derivatives are active components in functioning as membranes for water desalination experiments. Carbon materials derived from natural loofah sponge, such as biochar and activated carbons, are promising candidates for desalination. However, natural loofah sponge-based membrane water purification still has some drawbacks, which are given below.

- Higher cost for the membrane desalination set-up based on natural loofah sponge is a challenge, although the cost of natural loofah sponge is very low. Hence, developing a membrane assembly for water desalination experiments with low cost is necessary.
- Loofah is a tropical plant which requires a longer growing season and conditions of warm temperature. Hence, the natural loofah sponge has to be stored for use round the year. But aging leads to deterioration in mechanical integrity since it is composed of cellulose and other components. Hence, there is a requirement to develop a low-cost method to store natural loofah sponge.
- The preparation of composites/hybrids using natural loofah sponge and natural loofah sponge-derived materials with other active materials such as carbon nanotubes, graphene, *etc.* are less explored. Research has to be conducted in this direction to develop active membranes with high efficiency for water desalination application.
- Long-term cyclic performance is an issue for natural loofah sponge-based commercial water desalination membranes. The membranes should have long-term cyclic stability for industrial application. The performance of these membranes decreases after long-time usage. The addition of polymeric binders/adducts may help in increasing the cycle life.

By considering the above-mentioned drawbacks relating to the usage of natural loofah sponge and natural loofah sponge-derived materials, it is possible to use them as efficient futuristic materials for desalination applications. Hence utilization of these potential environmentally friendly materials for water desalination experiments will be an added advantage for sustainable means of scalable water purification with low cost.

5. Conclusions

In this review article, we have discussed the exemplary application of loofah sponge for wastewater desalination. Being a sustainable and environmentally friendly material with low cost, loofah sponge is a potential candidate for wastewater purification applications. The synthesis is scalable and large quantities of loofah sponge can be manufactured at a commercial scale, which points to the future marketing potential of this material.

Data availability

Data sharing not applicable – no new data generated. Data availability is not applicable to this article as no new data were created or analysed in this study.

Conflicts of interest

All authors declare no potential conflict of interest to report in relation to this work.

References

1 D. Bhanderi, P. Lakhani and C. K. Modi, Graphitic carbon nitride (gC_3N_4) as an emerging photocatalyst for sustainable environmental applications: a comprehensive review, *RSC Sustainability*, 2024, **2**, 265–287.
2 R. S. Pires, *et al.*, Elucidating the role of the nanostructure in protein aerogels for removal of organic water pollutants, *RSC Sustainability*, 2024, **2**(12), 4036–4045.
3 A. Ali, *et al.*, Covalent organic framework-based lamellar membranes for water desalination applications, *RSC Sustainability*, 2023, **1**(7), 1634–1654.
4 A. Adewuyi, *et al.*, Zeolitic imidazolate framework improved vanadium ferrite: toxicological profile and its utility in the photodegradation of some selected antibiotics in aqueous solution, *RSC Sustainability*, 2025, **3**, 427–439.
5 J. Cherusseri, *et al.*, SARS-CoV-2-on-chip for long COVID management, *Biosensors*, 2022, **12**(10), 890.
6 F. Ogata, *et al.*, Synthesis and characterization of the magnetic-carbonaceous materials from bamboo waste and investigation of its adsorption capability of cesium ions, *RSC Sustainability*, 2024, **2**, 2005–2014.
7 Y. Liu, *et al.*, Cuttlefish ink nanoparticles-integrated aerogel membranes for efficient solar steam generation, *RSC Sustainability*, 2024, **2**(2), 425–434.
8 S. A. Thomas, Layered two-dimensional black phosphorous-based hybrid electrodes for rechargeable batteries, *J. Energy Storage*, 2023, **73**, 109068.
9 S. A. Thomas, *et al.*, Strategically-Designed Environment-Friendly Tin-Based Electrodes for Sustainable Supercapatteries with High Specific Capacity, *Electrochim. Acta*, 2025, 145846.
10 J. Cherusseri, R. Sharma, and K. K. Kar, Nanotechnology advancements on carbon nanotube/polypyrrole composite electrodes for supercapacitors, *Handbook of Polymer Nanocomposites. Processing, Performance and Application: Volume B: Carbon Nanotube Based Polymer Composites*, 2015, pp. 479–510.
11 S. A. Thomas, *et al.*, Minireview on Exploring MAX Phases for Hydrogen Energy Storage: Strategies, Development, and Future Perspectives, *Energy Fuels*, 2025, **39**(3), 1460–1478.
12 D. Kumar, *et al.*, Nanocarbon assisted green hydrogen production: Development and recent trends, *Int. J. Hydrogen Energy*, 2024, **50**, 118–141.
13 S. Pramanik, *et al.*, Metal matrix composites: Theory, techniques, and applications, *Composite Materials: Processing, Applications, Characterizations*, 2017, pp. 369–411.
14 J. Cherusseri and K. K. Kar, Recent progress in nanocomposites based on carbon nanomaterials and electronically conducting polymers, *Polymer Nanocomposites Based on Inorganic and Organic Nanomaterials*, 2015, pp. 229–256.
15 S. A. Thomas and J. Cherusseri, Strategically designing layered two-dimensional SnS_2-based hybrid electrodes: A futuristic option for low-cost supercapacitors, *J. Energy Chem.*, 2023, **85**, 394–417.
16 S. A. Thomas, J. Cherusseri and D. N. Rajendran, Recent progresses in the synthesis and strategic designs of sustainable carbon-based fibrous electrodes for flexible batteries, *RSC Sustainability*, 2025, **3**, 219–242.
17 J. Cherusseri, *et al.*, Rapid synthesis of cobalt manganese phosphate by microwave-assisted hydrothermal method and application as positrode material in supercapatteries, *Sci. Rep.*, 2024, **14**(1), 26550.
18 M. Zaed, *et al.*, Hierarchical $Ti_3C_2T_x$ MXene@ Honeycomb nanocomposite with high energy efficiency for solar water desalination, *Chemosphere*, 2024, **366**, 143459.
19 M. Zaed, *et al.*, Unlocking desalination's potential: Harnessing MXene composite for sustainable desalination, *Chem. Eng. J.*, 2024, **500**, 156910.
20 M. Zaed, *et al.*, Synthesis of $Ti_3C_2T_x$ MXene@ Carbon-Enhanced cellulose fiber composite-based photothermal absorber for sustainable water desalination, *Mater. Today Sustain.*, 2024, **28**, 100971.
21 M. Zaed, *et al.*, Utilization of recycled materials for low-cost MXene synthesis and fabrication of graphite/MXene composite for enhanced water desalination performance, *Sep. Purif. Technol.*, 2025, **354**, 129055.
22 M. Zaed, *et al.*, Synthesis and characterization of hierarchical $Ti_3C_2T_x$ MXene/graphitic-carbon nitride/activated carbon@ luffa sponge composite for enhanced water desalination, *Open Ceram.*, 2024, **19**, 100645.
23 D. Curto, V. Franzitta and A. Guercio, A review of the water desalination technologies, *Appl. Sci.*, 2021, **11**(2), 670.
24 M. Zaed, *et al.*, Low-cost synthesis of $Ti_3C_2T_x$ MXene-based sponge for solar steam generation and clean water production, *Ceram. Int.*, 2024, **50**(16), 27910–27922.
25 S. N. Akhtar, *et al.*, Ionic polymer metal composites, *Composite Materials: Processing, Applications, Characterizations*, 2017, pp. 223–249.
26 R. Alrowais, *et al.*, A thermally-driven seawater desalination system: Proof of concept and vision for future sustainability, *Case Stud. Therm. Eng.*, 2022, **35**, 102084.
27 O. Shamet and M. Antar, Mechanical vapor compression desalination technology–A review, *Renewable Sustainable Energy Rev.*, 2023, **187**, 113757.
28 H. Yang, C. Yang and L. Geng, A heat pump-driven mechanical vapor compression desalination system and its operating characteristics, *Water Resour. Ind.*, 2024, **32**, 100264.
29 J. Eke, *et al.*, The global status of desalination: An assessment of current desalination technologies, plants and capacity, *Desalination*, 2020, **495**, 114633.
30 S. A. Thomas, *et al.*, Functionalized Carbon Nanostructures for Wastewater Treatments, in *Handbook of Functionalized Carbon Nanostructures: from Synthesis Methods to Applications*, Springer, 2024, pp. 1971–2014.
31 J. Cherusseri, *et al.*, Polymer-based composite materials: characterizations, *Composite Materials: Processing, Applications, Characterizations*, 2017, pp. 37–77.

32 M. Zaed, *et al.*, Synthesis of titanium carbide (TiC) using recycled precursor for potential scale-up of low-cost MXene, *Open Ceram.*, 2024, **19**, 100637.
33 S. A. Thomas, J. Cherusseri, and D. N. Rajendran, Functionalized Carbon Nanostructures for Hydrogen Storage, in *Handbook of Functionalized Carbon Nanostructures: from Synthesis Methods to Applications*, Springer, 2024, pp. 1471–1509.
34 S. A. Thomas, *et al.*, Graphitic Carbon Nitride and Their Derivatives, in *Handbook of Functionalized Carbon Nanostructures: from Synthesis Methods to Applications*, Springer, 2024, pp. 1–38.
35 J. Xu, *et al.*, Solar-driven interfacial desalination for simultaneous freshwater and salt generation, *Desalination*, 2020, **484**, 114423.
36 G. Liu, *et al.*, Salt-rejecting solar interfacial evaporation, *Cell Rep. Phys. Sci.*, 2021, **2**, 100310.
37 G. Yang, *et al.*, Janus hollow fibre membranes with intrusion anchored structure for robust desalination and leachate treatment in direct contact membrane distillation, *Desalination*, 2023, **551**, 116423.
38 J. Arnal, *et al.*, Concentration of brines from RO desalination plants by natural evaporation, *Desalination*, 2005, **182**(1–3), 435–439.
39 B. Richard, *et al.*, Minireview on fluid manipulation techniques for the synthesis and energy applications of two-dimensional MXenes: advances, challenges, and perspectives, *Energy Fuels*, 2023, **37**(10), 6999–7013.
40 M. M. Zubair, H. Saleem and S. J. Zaidi, Recent progress in reverse osmosis modeling: An overview, *Desalination*, 2023, **564**, 116705.
41 J. Yao, *et al.*, Interfacial solar evaporation for zero liquid discharge desalination, *Commun. Mater.*, 2024, **5**(1), 103.
42 Q. Zhang, *et al.*, High efficiency solar interfacial evaporator for seawater desalination based on high porosity loofah sponge biochar, *Sol. Energy*, 2022, **238**, 305–314.
43 Q. Zhang, *et al.*, Improving seawater desalination efficiency by solar driven interfacial evaporation based on biochar evaporator of Nannochloropsis oculata residue, *J. Environ. Chem. Eng.*, 2021, **9**(4), 105787.
44 S. A. Thomas, *et al.*, Translation of supercapacitor technology from laboratory scale to commercialization, in *Supercapacitors*, Elsevier, 2024, pp. 371–395.
45 J. Cherusseri, Polymer-Ionic Liquid Gel Electrolytes for Lithium-Ion Batteries, in *Polymer Electrolytes for Energy Storage Devices*, CRC Press, 2021, pp. 235–253.
46 S. A. Thomas, *et al.*, Water-in-salt electrolyte—toward high-voltage aqueous supercapacitors, in *Supercapacitors*, Elsevier, 2024, pp. 289–315.
47 J. Nallapureddy, *et al.*, Morphology controlled synthesis of $MnCo_2S_4$ nanoflower structures for different metal precursors used for energy storage applications, *J. Power Sources*, 2024, **613**, 234883.
48 M. R. Pallavolu, *et al.*, Scalable synthesis of binder-free hierarchical $MnCo_2O_4$ nanospikes/$Ni(OH)_2$ nanosheets composite electrodes for high-capacity supercapatteries, *J. Energy Storage*, 2023, **73**, 108999.
49 S. A. Thomas, *et al.*, Designing PEDOT-based hybrid electrodes for supercapacitors by electrospinning strategy, *Discover Electrochem.*, 2024, **1**(1), 6.
50 S. Abinaya, *et al.*, Unveiling dynamic insights of nitrogen-doped carbon quantum dots in α-Fe_2O_3/PANI nanocomposite for supercapattery application, *J. Mater. Sci.*, 2024, **59**(47), 21846–21867.
51 D. Mohan, C. Pittman Jr, and T. E. Mlsna, *Sustainable Biochar for Water and Wastewater Treatment*, Elsevier, 2022.
52 K. Sakuragi and M. Otaka, Effect of biomass carbonization on the grinding of coal/biomass mixtures, *ACS Omega*, 2020, **5**(34), 21722–21727.
53 J. de Siqueira Castro, *et al.*, Hydrothermal carbonization of microalgae biomass produced in agro-industrial effluent: Products, characterization and applications, *Sci. Total Environ.*, 2021, **768**, 144480.
54 J. Li, *et al.*, Pollen-derived porous carbon with excellent photothermal performance for laser ignition application, *Colloids Surf., A*, 2025, **707**, 135932.
55 R. Fillet, *et al.*, A review of natural materials for solar evaporation, *Sol. Energy Mater. Sol. Cells*, 2021, **219**, 110814.
56 Y. Chen, *et al.*, In-depth analysis of the structure and properties of two varieties of natural luffa sponge fibers, *Materials*, 2017, **10**(5), 479.
57 A. Ghaffar, *et al.*, Simultaneous solar steam and electricity generation from biochar based photothermal membranes, *J. Cleaner Prod.*, 2024, **446**, 141374.
58 X. Wang, *et al.*, A polyelectrolyte hydrogel coated loofah sponge evaporator based on Donnan effect for highly efficient solar-driven desalination, *Chem. Eng. J.*, 2023, **462**, 142265.
59 Q. Kong, *et al.*, Isotherm, kinetic, and thermodynamic equations for cefalexin removal from liquids using activated carbon synthesized from loofah sponge, *Desalin. Water Treat.*, 2016, **57**(17), 7933–7942.
60 Y. Yue, *et al.*, A loofah-based all-day-round solar evaporator with phenolic lignin as the light-absorbing material for a highly efficient photothermal conversion, *Chem. Eng. J.*, 2023, **477**, 147298.
61 C. Liu, *et al.*, An 'antifouling'porous loofah sponge with internal microchannels as solar absorbers and water pumpers for thermal desalination, *J. Mater. Chem. A*, 2020, **8**(25), 12323–12333.
62 Z. Qin, *et al.*, Janus biomass aerogel for Highly-Efficient steam Generation, Desalination, degradation of organics and water disinfection, *J. Colloid Interface Sci.*, 2023, **640**, 647–655.
63 C. Feng, *et al.*, Highly porous activated carbon with multi-channeled structure derived from loofah sponge as a capacitive electrode material for the deionization of brackish water, *Chemosphere*, 2018, **208**, 285–293.
64 D. Sriramulu, S. Vafakhah and H. Y. Yang, Activated Luffa derived biowaste carbon for enhanced desalination performance in brackish water, *RSC Adv.*, 2019, **9**(26), 14884–14892.
65 J. Wu, *et al.*, Hydrothermally modified 3D porous loofah sponges with MoS_2 sheets and carbon particles for efficient

solar steam generation and seawater desalination, *ACS Appl. Mater. Interfaces*, 2023, **15**(24), 29457–29467.

66 S. A. Thomas and J. Cherusseri, A Review of Nb_2CT_x MXene as an Emerging 2D Material: Synthesis, Applications in Rechargeable Batteries and Supercapacitors, Progress, and Outlook, *Energy Fuels*, 2023, **37**(11), 7555–7576.

67 S. A. Thomas, *et al.*, Boron carbon nitride (BCN): an emerging two-dimensional material for rechargeable batteries, *Energy Fuels*, 2024, **38**(15), 13704–13721.

68 D. Deng, *et al.*, Catalysis with two-dimensional materials and their heterostructures, *Nat. Nanotechnol.*, 2016, **11**(3), 218–230.

69 M. Zaed, *et al.*, Utilization of recycled materials for low-cost MXene synthesis and fabrication of graphite/MXene composite for enhanced water desalination performance, *Sep. Purif. Technol.*, 2024, 129055.

70 A. M. Saleque, *et al.*, MXene/MnO_2 nanocomposite coated superior salt-rejecting biodegradable luffa sponge for efficient solar steam generation, *Desalination*, 2023, **554**, 116488.

71 S. N. Farabi, *et al.*, RuO_2−MXene nanocomposite coated on bio-degradable loofah sponge for enhanced rate of evaporation in interfacial solar desalination, *Results Eng.*, 2024, **24**, 103450.

72 X. Jia, *et al.*, A loofah-based photothermal biomass material with high salt-resistance for efficient solar water evaporation, *Compos. Commun.*, 2023, **37**, 101430.